NASA TECHNICAL REPORT

NASA TR R-380

A HOLOGRAPHIC SYSTEM THAT RECORDS FRONT-SURFACE DETAIL OF A SCENE MOVING AT HIGH VELOCITY

by Robert L. Kurtz and H. Y. Loh

George C. Marshall Space Flight Center
Marshall Space Flight Center, Ala. 35812

TECH LIBRARY KAFB, NM

TECHNICAL REPORT

1. REPORT NO. NASA TR R-380	2. GOVERNMENT ACCESSION NO.	3. RECIPI 0068342
4. TITLE AND SUBTITLE A Holographic System That Records Front-Surface Detail of a Scene Moving at High Velocity		5. REPORT DATE January 1972
		6. PERFORMING ORGANIZATION CODE
7. AUTHOR(S) Robert L. Kurtz and H. Y. Loh *		8. PERFORMING ORGANIZATION REPORT #
9. PERFORMING ORGANIZATION NAME AND ADDRESS George C. Marshall Space Flight Center Marshall Space Flight Center, Alabama 35812		10. WORK UNIT NO. M442
		11. CONTRACT OR GRANT NO.
12. SPONSORING AGENCY NAME AND ADDRESS National Aeronautics and Space Administration Washington, D. C. 20546		13. TYPE OF REPORT & PERIOD COVERED Technical Report
		14. SPONSORING AGENCY CODE

15. SUPPLEMENTARY NOTES

* Professor, Physics Department, Virginia Polytechnic Institute

16. ABSTRACT

It is known that any motion of the scene during the exposure of a hologram results in a spatial modulation of the recorded fringe contrast. On reconstruction this produces a spatial amplitude modulation of the reconstructed wavefront that tends to blur out the image. This report discusses a novel holographic technique that uses an elliptical orientation for the holographic arrangement. It is shown that the degree of image degradation is not only a function of exposure time but also of the system used. The form of the functional system dependence is given, as well as the results of several systems tested, which verify this dependence. It is further demonstrated that the important parameter is the total motion of the target $\Delta X = VT$. Using the experimentally determined resolution of front-surface detail from a target with a velocity of 17 546 cm/s, an upper limit on target velocity for resolution of front-surface detail for a given system can be predicted.

17. KEY WORDS Holography Motion Holography Motion Picture Holography Moving Scene Holography Hypervelocity Holography	18. DISTRIBUTION STATEMENT

19. SECURITY CLASSIF. (of this report) Unclassified	20. SECURITY CLASSIF. (of this page) Unclassified	21. NO. OF PAGES 96	22. PRICE $3.00

TABLE OF CONTENTS

TABLE OF CONTENTS (Concluded)

LIST OF ILLUSTRATIONS

LIST OF ILLUSTRATIONS (Concluded)

LIST OF TABLES

DEFINITION OF SYMBOLS

Symbol	Definition
a	Semimajor axis of ellipse
$a(x, y)$	Amplitude function of reference field
b	Semiminor axis of ellipse
$b(x, y)$	Amplitude function of scene field
d	Separation distance from foci to origin of ellipse
E_r	Reference field
E_s	Scene field
E_t	Transmitted field
$\mathscr{E}$	Exposure
I	Intensity of irradiance $\equiv m\,|E|^2$
m	A constant $\equiv \dfrac{1}{2Z}$
$\bar{S}_i$	Average measurement of length of image resolved
$\bar{S}_{0_i}$	Relative average length $= \dfrac{\bar{S}_i \text{ (motion case)}}{\bar{S}_i \text{ (stationary case)}}$
T	Transmission coefficient
T_a	Transmission amplitude coefficient
v	Magnitude of velocity

LIST OF SYMBOLS (Concluded)

$\vec{V}$ Velocity vector

Z Impedance $= \sqrt{\dfrac{\mu}{\epsilon}}$

α Phase function of reference field

β Phase function of scene field

γ Contrast of photographic film or plate

ΔL Total change in optical pathlength of front illumination beam

τ Time

ACKNOWLEDGEMENTS

A HOLOGRAPHIC SYSTEM THAT RECORDS FRONT-SURFACE DETAIL OF A SCENE MOVING AT HIGH VELOCITY

I. INTRODUCTION

In 1947, Dr. Dennis Gabor of the University of London coined the word "hologram," which means entire word or whole picture. Holography is a two-step imaging process that involves the recording of an interference pattern usually between two beams from a common origin and the subsequent use of this recorded pattern to construct an image of the original object.

From the physical arrangement of the separated light beams (the modulated signal beam and the unmodulated reference beam), one is able to record not only the amplitude but also the phase of the light beam as well. The medium normally used for the recording is conventional photographic emulsions. Herein, the primary difference lies between holography and conventional photography — the ability to record phase of the light as well as amplitude while using essentially the same type of square law detector.

The light intensity recorded by the photographic film or spectroscopic plate is a function of the amplitude of the wave from the object or signal beam and the amplitude of the unmodulated or reference beam. Since interference between these two waves at the film plane exists, the two waves interact here and provide a maximum intensity where the crests of both waves meet and a minimum where the crest of one meets the trough of the other. This interaction of the two light waves forms lines of exposure on the photographic emulsion. As each point on the object contributes its share of lines or fringes, all of the optical information about the object is stored on the plate.

Remembering that the fringes dictate the position of each object point as it relates to the unmodulated reference beam, illumination of the processed film with the reference beam alone will reconstruct the original signal beam and an image of the original object will appear in the same position as the original object; it will be quite authentic but slightly reduced in brightness. Since forming a holographic recording is essentially a two-beam interference experiment, it is important that the phase difference between the two beams remains essentially constant during the exposure. A change in the path difference at the recording plane of $\lambda/2$ (λ is the wavelength of illumination being used) will shift the fringe position by one-half of one fringe spacing. If this shift occurs during the exposure, the recorded fringe modulation will fall to essentially zero and it is possible that no hologram will be recorded. Such

path-length changes or phase shifts can be caused by numerous situations; for example, vibration of the optical components, creep or vibration of the emulsion of the film plane, or motion of the object under test. However, it is suggested that object motion with time dependence and magnitude will be recorded by the hologram if the location and orientation of the holographic system are properly chosen.

The purpose of this report is to discuss one such proper location. It is a new holographic technique that offers promise for the holographic recording of front-surface detail from an object traveling in an essentially straight line with constant velocity of very high magnitude. A simple analysis, given in Section IV, shows that this technique is capable of recording front-surface detail from a moving scene traveling at very high velocities, depending upon the pulse duration of the laser source, its power output, and the tolerance of the optical path difference.

This subject of motion holography has covered scenes from microscopic particles and aerosol sprays to seeded gas flow and bullet-type projectiles. The bullet-type or macroscopic projectiles have received considerable attention recently. A reasonable search of the literature by the author revealed that the highest target velocity for which a hologram was successfully recorded was 375 m/s [1]. However, no report of the resolution of front-surface detail from targets at high speeds was found. According to the calculations made in Section IV.A, the technique will allow resolution of front-surface detail from a moving scene having a velocity of 9×10^5 cm/s, using a 25-ns pulse-length ruby laser, and still not cause the path length change of the signal beam to be greater than $\lambda/8$ (phase shift $\pi/4$). As will be shown later, this small phase shift cannot be accounted for on the basis of the pulse length or exposure time alone; i. e., the resultant shift is also system dependent.

This report first defines a variety of types of holography, and then derives detailed theory of one type of holography in particular — Fresnel sideband holography — since this is the type of holography utilized in the experimental testing of the present technique. It is also shown that holographic recording of the resolution of front-surface detail for scenes moving at high velocities is possible; it presents experimental evidence of this for a given total scene travel, Δx, since the primary parameter is just the total motion, Δx, that the scene undergoes during the exposure. The appendix gives the role of photography in the holographic process.

Furthermore, since the effect of the scene motion on a hologram and its reconstructed image is the summation of the effects resulting from each point of the scene contributing individually, such motion-induced effects of a single point of the scene will be considered; then, one may obtain the complete field by the principle of superposition.

2

II. LITERATURE REVIEW

An extensive computerized literature search of the general area of holography yielded more than 400 reference sources for holography. Many of these sources concern specialized applications and varied types of holography. Those pertinent to this application have been included in the References and Bibliography.

In this literature review, emphasis is placed on those reference sources dealing primarily with motion holography (either motion of the scene or of the components). No reference has been found in which the resolution of front-surface detail was experimentally obtained from a moving scene at velocities higher than a few centimeters per second. However, as indicated in the Introduction, a number of researchers agree that this type of resolution can theoretically be obtained if proper system orientation is found for a given type of motion.

Initially, this review will present the four basic types of holography from which additional variations can be, and have been, made and the essential requirements of each. These four types of holography are as follows:

(a) CONSTRUCTION

(b) RECONSTRUCTION
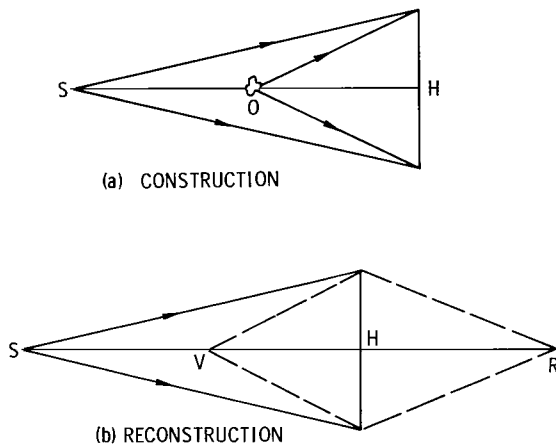
Figure 1. Gabor in-line holography

1. The Gabor in-line type of holography is shown in Figure 1a. A divergent beam from the source, S, is incident on an object, O, or scene, on the optical axis and also passes around the object on all sides to form the unmodulated reference beam for this arrangement. Obviously, the first limitation of this system is on the object size. The next limitation is on the resolving power since the reference waves and the scattered rays cross at a small angle to give coarse fringes (see Appendix). The next, and perhaps primary, limitation is because the object and source fall on the optic axis and, hence, the term "in-line;" in the reconstruction (Fig. 1b), when a real image, R, and virtual image, V, are produced, they are essentially in a straight line. For this reason, it is almost impossible to separate them except by complex procedures. The advantage of this arrangement is the system's

requirement of low resolution that allows the use of coarse-grained and, therefore, fast film. Furthermore, this system shows greater tolerance to a lack of mechanical stability.

2. Direct-transmission holography or dark-field holography is quite applicable to the aerodynamic study of the behavior of fluid or gas flow fields. An example of this type of holography arrangement is shown in Figure 2, which utilizes a modified Mach-Zender interferometer [2].

3. Diffuse-transmission holography is very similar to the direct-transmission method except that now a diffusing screen is placed in the signal beam upstream of the object (Fig. 3). If direct transmission is called dark-field holography, then diffuse transmission is called light-field holography. This is because this type of holography recreates the diffuse screen, which acts as a luminous background against which the object appears in silhouette. Thus, viewing can be done with the unaided eye instead of with an eyepiece or screen as is necessary for the first two methods. The main advantage of this method is to avoid the high sensitivity to disturbance by dust particles inherent in the previous methods [2]. This method is most adaptable to the holography of moving targets and allows a black silhouette of the traveling target against a lighted diffuser background. This method has been used almost unanimously for motion holography studies [3, 4, 5, 6, 7, 8, 9, 10, 11].

4. Reflection holography has many of the characteristics of diffuse-transmission holography with the advantage that the object is illuminated from the front or from one side, rather than from behind, and, consequently, provides resolution of front-surface detail. An arrangement for both producing and reconstructing the reflection-type hologram is shown in Figure 4. The requirements of this system for mechanical stability are quite severe. The resolution requirement is strictly a function of the angle between the signal and reference beam at the holographic plate (see Appendix).

With the exception of the Gabor type, all the other arrangements may be grouped into the Fresnel sideband holographic category. There is a category called the Fourier Transform Holography [2, 9, 12, 13, 14, 15, 16], whose component arrangement is given in Figure 5. This arrangement provides a means of storing the information in an assembly of straight-line fringes lying at different angles across the plate and having different spacings. This has such applications as information storage and pattern recognition. The present system described in Section IV is basically a Fresnel sideband form of holography and utilizes type 4 in a modified version.

4
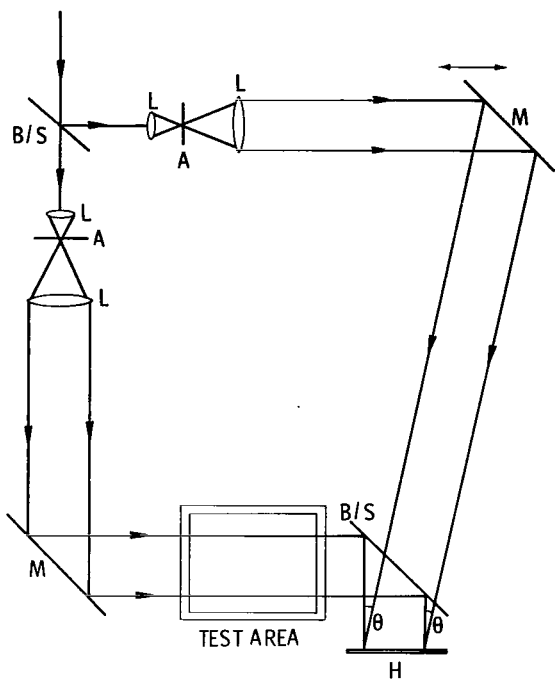
Figure 2. Direct-transmission
holography
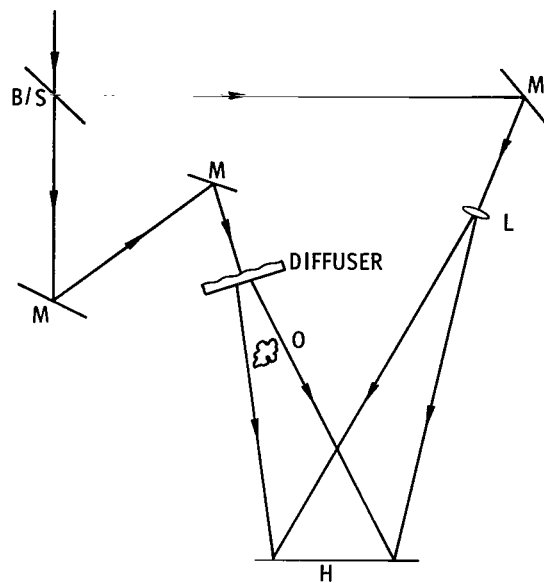
Figure 3. Diffuse-transmission
holography
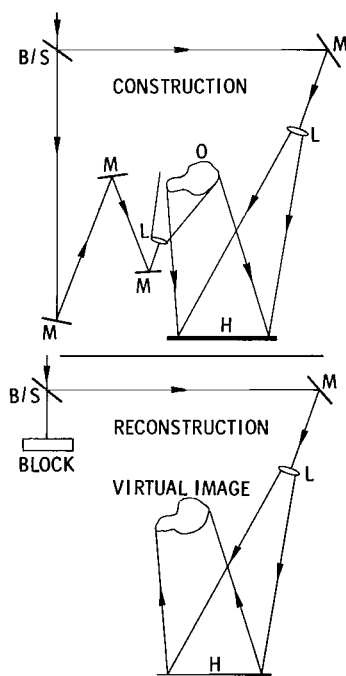
Figure 4. Front surface
reflection holography
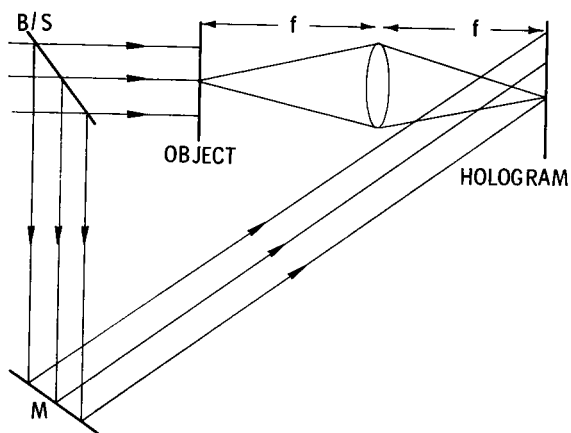
Figure 5. Fourier transform
holography

Many experimenters have produced holograms of high-speed phenomena using either type 3, the diffuse-transmission arrangement where the scene appears in silhouette against some lighted background, or type 2, the direct-transmission or dark-field holography [2, 3, 4, 5, 6, 7, 8, 9, 10, 11, 17, 18]. Some success has been accomplished using the far-field or Fraunhofer-type holography [19]; whereas, some experimenters have applied the Fourier transform holography to velocity determination of scenes [12]. Although the preceding references demonstrate the ability to holograph motion quite successfully, none to date have achieved front-surface resolution from these moving scenes [20, 21, 22, 23, 24, 25, 26, 27]. Some measure of success has been shown in obtaining front-surface resolution from moving targets but only at extremely low velocities or at apparent velocities; i. e., animation [1, 8]. The ability to holographically achieve resolution of front-surface detail from fast-moving scenes has been demonstrated in Section IV. The final purpose of this report is to produce a means of demonstrating this feat experimentally.

III. THEORY OF HOLOGRAPHY

A. A General Description of Fresnel Sideband Holography for a Stationary Scene

Let the plane of the hologram lie in the x-y plane of the coordinate system as given in Figure 6. The amplitude in this plane can be described by the radiation from the scene,

$$E_s = b(x, y) \exp\{i[\beta(x, y) - \omega t]\} \quad , \quad (1)$$

and by that of the reference beam,

$$E_r = a(x,y) \exp\{i[\alpha(x, y) - \omega t]\} \quad . \quad (2)$$

The amplitude functions $b(x, y)$ and $a(x, y)$ and the phase functions $\alpha(x, y)$ and $\beta(x, y)$ are considered here to be real functions. This, then, is a scalar treatment that does not take account of polarization effects. However, it is always possible to split the scene wave into two components, one with the electric vector in the plane containing the electric vector and the direction of propagation of the reference ray and the other with the electric vector perpendicular to this plane. Only the

Figure 6. Hologram coordinate system for stationary scene

parallel component contributes to the interference pattern on the hologram and, hence, to the reconstruction. Furthermore, a(x, y) is a slowly variable function (a constant for a plane reference wave, but, for a spherical wave, it varies as the reciprocal of distance from the reference source to different points on the hologram). The reference wave may also be a distorted spherical wave, as formed by a lens with geometrical aberrations. The amplitude function of the scene (object) wave, b(x, y), is materially smaller than a(x, y), since the ratio of intensity of the reference beam to that of the scene beam is usually required to be 10 to 1. The exposure on the hologram plate is given by the product of intensity at the plate times the time of exposure, or pulse length.

In general, from the definition of Poynting's vector in the rationalized mks system,

$$\vec{S} \equiv \vec{E} \times \vec{H} \quad ,$$

one can see that its time average is

$$\langle \vec{S} \rangle = \langle \vec{E} \times \vec{H} \rangle = 1/2 \sqrt{\frac{\epsilon}{\mu}} \quad EE^* \quad \hat{n} \quad , \tag{3}$$

where E^* is the complex conjugate of E and $\hat{n}$ is a unit vector, mutually perpendicular to $\vec{E}$ and $\vec{H}$. Since the intensity (i. e., irradiance) of electromagnetic radiation is the energy crossing normal to a unit area per unit time,

$$I = \langle S \rangle = 1/2 \sqrt{\frac{\epsilon}{\mu}} \quad EE^* = 1/2Z \, EE^* \equiv m \, EE^* \quad , \tag{4}$$

where $Z = \sqrt{\frac{\mu}{\epsilon}}$ is the impedance of the medium and m is a constant for simplification. For a hologram,

$$I = m \, EE^* = m(E_r + E_s) \, (E_r^* + E_s^*), \tag{5}$$

and, from equations (1) and (2),

$$I = m \left\{ b(x, y) \, e^{i[\beta(x, y) - \omega t]} + a(x, y) \, e^{i[\alpha(x, y) - \omega t]} \right\}$$

$$\cdot \left\{ b(x, y) \, e^{-i[\beta(x, y) - \omega t]} + a(x, y) \, e^{-i[\alpha(x, y) - \omega t]} \right\} \tag{6}$$

7

or

$$I = m \left(b^2(x, y) + a^2(x, y) + a(x, y)\, b(x, y) \left\{ e^{i[\beta(x, y) - \alpha(x, y)]} + e^{-i[\beta(x, y) - \alpha(x, y)]} \right\} \right) , \tag{7}$$

where equation (7), for the intensity recorded at the plate, is generally called the recording equation.

Now substitution of equation (7) into the equation for the exposure produces

$$\mathcal{E} = \int_0^\tau I\, dt = m \int_0^\tau b^2(x, y) + a^2(x, y) + 2a(xy)\, b(xy) \cos(\beta - \alpha)\, dt$$

or

$$It = m\tau \quad b^2(x, y) + a^2(x, y) + 2a(x, y)\, b(x, y) \cos(\beta - \alpha) \tag{8}$$

but τ is just some constant exposure time, τ_0, for a given hologram; therefore, the exposure may be simply written as

$$It = m\tau_0 \left[a^2 + b^2 + 2ab \cos(\beta - \alpha) \right] ,$$

where a, b, α, and β are coordinate dependent, or

$$It = m\tau_0 \left\{ a^2 + b^2 + ab \left[e^{i(\beta - \alpha)} + e^{-i(\beta - \alpha)} \right] \right\} \tag{9}$$

It is well known in photography [28] that the Heurter-Driffield characteristic curve as plotted on a semilog plate (Appendix, Fig. A-2) is linear for most of its length and can be represented in this linear region by:

$$D = \gamma \log\frac{I\tau}{g} ,$$

where D is the density of the image on the film, γ is the contrast, and g is the inertia of the emulsion. Since

$$D \equiv -\log T,$$

$$T = g^\gamma (I\tau)^{-\gamma} , \tag{10}$$

8

where T is the transmission coefficient. The amplitude transmission coefficient, T_a, is the square root of the transmission; consequently,

$$T_a = g^{\gamma/2} (I\tau_0)^{-\gamma/2} = k \, I^{-\gamma/2} \quad , \tag{11}$$

where $k \equiv (g/\tau_0)^{\gamma/2}$ is a constant and

$$T_a = k \left[a^2 + b^2 + ab \left(e^{i(\beta - \alpha)} + e^{-i(\beta - \alpha)} \right) \right]^{-\gamma/2} ; \tag{12}$$

factoring,

$$T_a = (k) \, (a^2 + b^2)^{-\gamma/2} \left[1 + \frac{a \, b}{a^2 + b^2} \left(e^{i(\beta-\alpha)} + e^{-i(\beta-\alpha)} \right) \right]^{-\gamma/2} . \tag{13}$$

Binomial expansion may be used to get

$$T_a = k(a^2 + b^2)^{-\gamma/2} \left[1 - \frac{\gamma}{2} \frac{a \, b}{a^2 + b^2} \left(e^{i(\beta - \alpha)} + e^{-i(\beta - \alpha)} \right) \right. $$
$$\left. + \text{higher-order terms} \right] \quad . \tag{14}$$

However, by careful development of the exposed plate, one obtains a positive transparency with an overall gamma of $(\gamma = -2)$, which yields

$$T_a = k(a^2 + b^2) \left[1 + \frac{a \, b}{a^2 + b^2} \left(e^{i(\beta-\alpha)} + e^{-i(\beta-\alpha)} \right) \right] \tag{15}$$

and higher-order terms are omitted because they are negligibly small compared to 1.

Consider the usual case where the reference beam during reconstruction is essentially identical with that during recording. Let this reference wave be incident on the developed hologram; just beyond the hologram the wave amplitude is

$$E_t = T_a E_r \quad . \tag{16}$$

9

Then, from equations (2) and (15),

$$E_t = \left[ka(a^2 + b^2) \right] \left[e^{i(\alpha - \omega t)} + \frac{a\,b}{a^2 + b^2} \left(e^{i(\beta - \omega t)} + e^{-i(\beta - 2\alpha + \omega t)} \right) \right] \quad . \tag{17}$$

The first term,

$$ka(a^2 + b^2)\, e^{i(\alpha - \omega t)} \quad , \tag{18}$$

is then simply the reference beam attenuated by a term proportional to $(a^2 + b^2)$; therefore, the first term is

$$k(a^2 + b^2)\, E_r \quad . \tag{19a}$$

The second term,

$$\left[ka(a^2 + b^2) \right] \left[\frac{a\,b}{a^2 + b^2}\, e^{i(\beta - \omega t)} \right] \quad , $$

becomes

$$ka^2 \left(b\, e^{i(\beta - \omega t)} \right) = k\, a^2\, E_s \quad , \tag{19b}$$

which corresponds to the original wave, equation (1) multiplied by the same shading factor as for the reference beam. One may infer from the form of the second term that on viewing through the hologram, illuminated by the reference beam, one should see this virtual image of the object in the precise position previously occupied by the object with reference to the original position of the hologram. If the hologram is in its same position after reconstruction, the image of the object will be precisely superimposed on the actual object. However, the brightness of the image will be slightly reduced.

The third term,

$$k\, a^2\, b\, e^{-i(\beta - 2\alpha + \omega t)} = k\, a^2\, b\, e^{i2(\alpha - \beta)\, +\, i(\beta - \omega t)} \quad ,$$

becomes

$$k\, a^2\, e^{i2(\alpha - \beta)}\, E_s \quad , \tag{19c}$$

10

which corresponds to the real image of the object and is located on the opposite side of the hologram plate from the virtual image. This real image is not aberration-free and is therefore termed "pseudoscopic."

B. The Effect of Linear Scene Motion During the Hologram Exposure

The effect of scene motion during the exposure of a hologram is a spatial modulation of the recorded fringe contrast. This, in turn, causes a spatial amplitude modulation of the reconstructed wavefront that blurs the reconstructed image in the same way that it would blur a conventional photograph having the same exposure time. In addition, this modulation reduces the brightness of even that part of the image that is reconstructed. The amount of object motion that can be successfully tolerated during the hologram exposure is certainly dependent upon the geometry of the holographic configuration with respect to the velocity vector of the motion. One such chosen geometry is discussed in detail in Section IV.

Two different theoretical approaches to the time-dependent theory of motion holography will be presented which follow closely the methods presented by Neumann [16]. Both approaches serve a purpose. The first uses a coordinate system with origin at the scene point of interest, which is a vector approach that allows a more intuitive feeling for the physics of the problem. It is primarily valid only for those cases where the allowed motion is small compared with the distance from the scene to the hologram. This particular approach is applied to the present system under investigation in Section IV. The second approach uses a coordinate system with the origin at the hologram. It is the most general derivation, and if a sufficient number of terms are taken in the infinite series that occurs, it will cover all geometries. It suffers, however, from the mathematical complexity that results from these expansions.
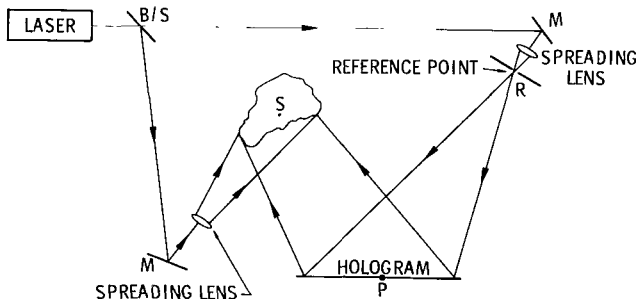
Figure 7. Typical configuration

1. Scene-Oriented Coordinates. Following Neumann, a basic holographic configuration is assumed (Fig. 7).

The radiation from the laser is split into two beams. As usual, these are considered to be the reference beam and the signal beam. Let the point R of Figure 7 serve as the reference position for the system and S be some point of the scene. Light scattered from point S is made incident at the point P of the hologram, where it now interferes with light from the reference point.

Let the field at point P be given by

$$\vec{E}(P) = \vec{E}_r(P) + \vec{E}_s(P)$$

or

$$E(P) = E_r(P)\, e^{i[\omega t - kr(P)]} + E_s(P)\, e^{i[\omega t - ks(P)]} \quad , \qquad (20)$$

where $\vec{E}_r(P)$ is the contribution from the reference point and is considered to be plane polarized, $\vec{E}_s(P)$ is the contribution at P because of the scene point, S, and is the component of the scene-field parallel to the reference polarization, and r and s are the corresponding pathlengths from the laser to the point P.

Now, the intensity is given by

$$I = m\,|E\,|^2$$

Therefore,

$$I = m\left[E_r^2 + E_s^2 + 2E_r E_s \cos k(r-s)\right] \quad . \qquad (21)$$

If the point, S , is allowed to move with some velocity, then s becomes a function of time. It is assumed, however, that the field amplitude does not change appreciably over the time, τ, of the exposure. Thus, the interference pattern remains approximately constant except for the motion of the fringes.

Then as before, the exposure can be written as

$$\mathcal{E}(P) = m \int_{-\tau/2}^{\tau/2} \left\{ E_r^2 + E_s^2 + 2E_r E_s \cos k[s(t) - r] \right\} dt$$

and

$$\mathcal{E}(P) = m\,\tau \left\{ E_r^2 + E_s^2 + \frac{2E_r E_s}{\tau} \int_{-\tau/2}^{\tau/2} \cos k\,[s(t) - r]\, dt \right\} \quad .$$

12

Let

$$K_C = E_r{}^2 + E_s{}^2$$

and

$$\mathscr{E}(P) = m\tau \left\{ K_C + \frac{2E_r E_s}{\tau} \int_{-\tau/2}^{\tau/2} \cos k[s(t) - r]dt \right\} \quad . \tag{22}$$

To proceed, the time dependence of s must be given. In general, $s = s_0 + f(t)$ where $f(t)$ may be any function of time where the midpoint of the exposure is at $\tau = 0$.

In particular, if it is assumed that s varies linearly with time, one has

$$s = s_0 + vt \quad ;$$

then equation (22) becomes

$$\mathscr{E}(P) = m\tau \left\{ K_C + \frac{E_r E_s}{\tau/2} \int_{-\tau/2}^{\tau/2} \cos[kvt + k(s_0 - r)]dt \right\} . \tag{23}$$

Let $\Phi = k(s_0 - r)$ be the time invariant portion; then

$$\mathscr{E}(P) = m\tau \left[K_C + \frac{E_r E_s}{\tau/2} \int_{-\tau/2}^{\tau/2} \cos(kvt + \Phi)\, dt \right] \tag{24}$$

after integration:

$$\mathscr{E}(P) = m\tau \left(K_C + E_r E_s \frac{\sin kv\,\tau/2}{kv\,\tau/2} \cos \Phi \right) \quad . \tag{25}$$

Then, since $\dfrac{\sin x}{x} = \operatorname{sinc} x$, one obtains for the exposure

$$\mathscr{E}(P) = m\tau \left[K_C + E_r E_s \operatorname{sinc}(kv\,\tau/2) \cos \Phi \right] \quad . \tag{26}$$

If v = 0, then no motion exists (i. e., the stationary case), and the sinc function becomes unity. This is the most desired case for most holographic experiments; i. e., that the argument of the sinc function be zero.

It is observed that if v is constant over the hologram, the resulting fringe contrast of the exposure will be poor for large values of the sinc argument and the resulting fringe contrast will be zero whenever the argument is $n \pi$ ($n = \pm 1, 2 \ldots$). Consider, for example, $n = 1$, where the first zero occurs; then,

$$\frac{kv \tau}{2} = \pi \tag{27}$$

or

$$v \tau = \lambda \quad . \tag{28}$$

Now, since $v\tau$ is the change in the distance, s, during the exposure, the possibility exists that motions of the scene as small as a wavelength may totally destroy the fringes or, at best, result in a poor hologram.

Fortunately, v is not the same for all points of the hologram and the fringe contrast is spatially modulated rather than destroyed [29].

This special case of the linear time variation of s has served to demonstrate the sinc function modulation of the recorded fringes. The problem may now be discussed with respect to the velocity vector of the motion. Consider the diagram in Figure 8, where R is the reference point and, as before, S is the scene point. Let L be a point on some reference phase front from the laser, which will be common to both beams. Let $\hat{a}_k$ be the unit vector along the direction of propagation of the incident laser radiation at the scene point, S, $\hat{a}_p$ be a unit vector along the line from scene point, S, to hologram point P, and $\hat{a}_v$ be a unit vector indicating the velocity of the scene point, S.

Figure 8. General geometry for scene–oriented coordinates

The reference beam is constant in length and composed of two parts, LR + RP. The front illumination beam or scene beam is composed of the two parts, LS + SP. The rate of change of the path length, LS, from the laser to the scene point, S, is given by

$$\vec{V} \cdot \hat{a}_k = v \cos \gamma \quad .$$ (29)

The rate at which the path length, SP, from the scene point to the hologram point, P, changes is given by

$$\vec{V} \cdot \hat{a}_p = v \cos \delta \quad .$$ (30)

Therefore, the path length from the laser to the hologram point, P, through scene point, S, is increasing at the rate

$$\frac{ds}{dt} = (\vec{V} \cdot \hat{a}_k - \vec{V} \cdot \hat{a}_p) \quad ,$$ (31)

$$\int_{s_0}^{s} ds = \int_{-\tau/2}^{\tau/2} \vec{V} \cdot (\hat{a}_k - \hat{a}_p) \, dt \quad ,$$ (32)

and

$$s = s_0 + \vec{V} \cdot (\hat{a}_k - \hat{a}_p)\tau \quad .$$ (33)

However, recall that, in general,

$$s = s_0 + f(t) \quad ,$$ (34)

and, in the special case considered previously,

$$s = s_o + vt \quad ;$$ (35)

therefore,

$$v = \vec{V} \cdot (\hat{a}_k - \hat{a}_p) \quad .$$

One may write the sinc function for this case as

$$\text{sinc}\left[\frac{k\tau v}{2} \ \hat{a}_v \cdot (\hat{a}_k \cdot \hat{a}_p)\right] \quad . \tag{36}$$

Thus, the exposure at the hologram point, P, for this case becomes

$$\mathscr{E}(P) = m\tau \left\{ K_C + E_r E_s \ \text{sinc}\left[\left(\frac{k\tau v}{2}\right)\hat{a}_v \cdot (\hat{a}_k - \hat{a}_p)\right] \cos \Phi \right\} \quad . \tag{37}$$

Looking again at the sinc function of equation (36) and performing the indicated scalar products, one sees that

$$\text{sinc}\left[\frac{k\tau v}{2} \ \hat{a}_v \cdot (\hat{a}_k - \hat{a}_p)\right] = \text{sinc}\left[\left(\frac{k\tau v}{2}\right)(\cos \gamma - \cos \delta)\right] \quad . \tag{38}$$

In this form, the modifying function allows several facts to be noted by inspection. Except for the case of $\tau v = 0$ (i. e., stationary scene, because sinc $0 = 1$), the sinc function has a maximum for only the following conditions:

1. The condition in which $\hat{a}_k$ is parallel to $\hat{a}_p$.

2. The condition where $\vec{V}$ is perpendicular to the vector $(\hat{a}_k - \hat{a}_p)$.

Consider that the vector $\hat{a}_p$ always points toward the hologram plane (whatever its position); then, the condition that $\hat{a}_k$ and $\hat{a}_p$ be parallel can only be met if $\hat{a}_k$ also points toward the hologram. It is seen that this condition is equivalent to the arrangement for the direct- and diffuse-type holography described earlier. This maximum occurs at the point where the incident laser radiation intersects the hologram plane when projected through the scene point. It is noted that the sinc function is a maximum for all orientations of the motion vector, $\vec{V}$.

The second condition for a maximum, that $(\hat{a}_k - \hat{a}_p)$ always be perpendicular to the motion vector $\vec{V}$, is satisfied for all vectors $(\hat{a}_k - \hat{a}_p)$ lying in a plane perpendicular to $\hat{a}_v$, since, for that condition,

$$\vec{V} \cdot (\hat{a}_k - \hat{a}_p) = 0 \quad ; \tag{39}$$

16

but,

$$\vec{V} \cdot (\hat{a}_k - \hat{a}_p) = v(\cos \gamma - \cos \delta) = 0 , \qquad (40)$$

and this condition is satisfied whenever $\delta = \pm \gamma$. (It should be noted that this condition is precisely satisfied by the system described in Section IV.A.) This condition is met by any vector, $\hat{a}_{p_0}$, making an angle, γ, with the vector, $\hat{a}_v$. The locus of these vectors, $\hat{a}_p$, forms a circular cone with a half angle equal to γ about the motion vector and contains $\hat{a}_k$ as an element (Fig. 9).

PLANE OF CONE BASE ⊥ TO $\vec{v}$

$\hat{a}_{po}$, TYPICAL VECTOR

γ

$\vec{v}$

$\hat{a}_k$

LOCUS OF VECTORS $\hat{a}_p$

Figure 9. Cone of constant fringe contrast
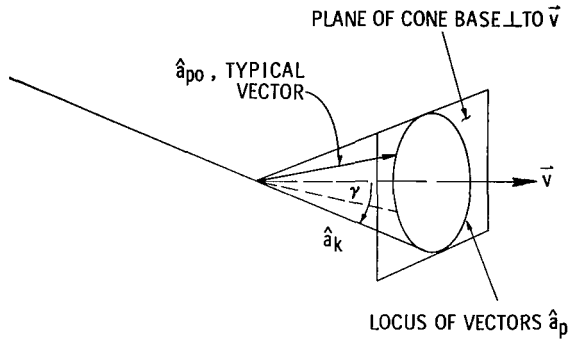
The zeros of the sinc function, equation (38), occur for

$$\text{sinc} \left[\frac{\tau k \vec{V}}{2} \cdot (\hat{a}_k - \hat{a}_p) \right] = \text{sinc } n\pi \qquad (41)$$

$$n = \pm 1, 2 . . .$$

Therefore, the zeros occur for

$$\frac{\tau k \vec{V}}{2} \cdot (\hat{a}_k - \hat{a}_p) = n\pi \quad ; \quad (42)$$

i. e.,

$$\vec{V} \cdot (\hat{a}_k - \hat{a}_p) = \frac{2n\pi}{\tau k} \qquad (43)$$

or

$$\hat{a}_v \cdot (\hat{a}_k - \hat{a}_p) = \frac{n\lambda}{v \tau} , \qquad (44)$$

and

$$\cos \gamma - \cos \delta_{n\pi} = \frac{n\lambda}{v \tau} \qquad (45)$$

or

$$\cos \delta_{n\pi} = \cos \gamma - \frac{n\lambda}{v \tau} , \qquad (46)$$

where $\delta_{n\pi}$ is that angle between vectors $\hat{a}_{p_0}$ and $\hat{a}_v$ which produces a zero value for the sinc function (i. e., that angle where no fringes will be recorded).

From the above and Figure 9, it is obvious that if a hologram is formed at any point in space, regions of the hologram having constant fringe contrast will form a conic section, since they represent the intersection of the hologram plane and the conical loci mentioned above. If the vector $\hat{a}_p$ is allowed to take on various values, δ, in the range

$$\gamma \leq \delta \leq \gamma + 2\pi \tag{47}$$

for a constant $\hat{a}_k$ with angle γ, one can then construct all possible orientations of $\hat{a}_p$ about the motion vector, $\vec{V}$. If for each specific value of δ one allows it to rotate about the velocity vector, $\vec{V}$, then one is able to construct all possible conical loci for $\hat{a}_p$. The results of this are shown in Figure 10 where three possible values of γ for $\hat{a}_k$ and all possible values of δ for $\hat{a}_p$ for the specific γ are taken. The values of the argument of the sinc function for $\gamma = 0$, $\pi/4$, and $\pi/2$ are then plotted.

2. Hologram-Oriented Coordinates. In the development of the previous subsection, the exposure is given by

$$\mathcal{E}(P) = m\tau \left\{ K_c + \frac{2E_r E_s}{\tau} \int_{-\tau/2}^{\tau/2} \cos k[s(t) - r] \, dt \right\} \ . \tag{48}$$

As before, the form of $s(t)$ must be determined, but now as a function of the hologram.

For this development, a fixed-coordinate system is used which has origin at the center of the hologram and the Z-axis normal to the plane of the hologram. This approach or development is the most generalized derivation, since it may be used for the region near the hologram as well as the region far from the hologram by simply taking a sufficient number of terms in the series expansions that are developed. Its primary malady is that these very expansions tend to obscure the physical significance of the various steps.

18
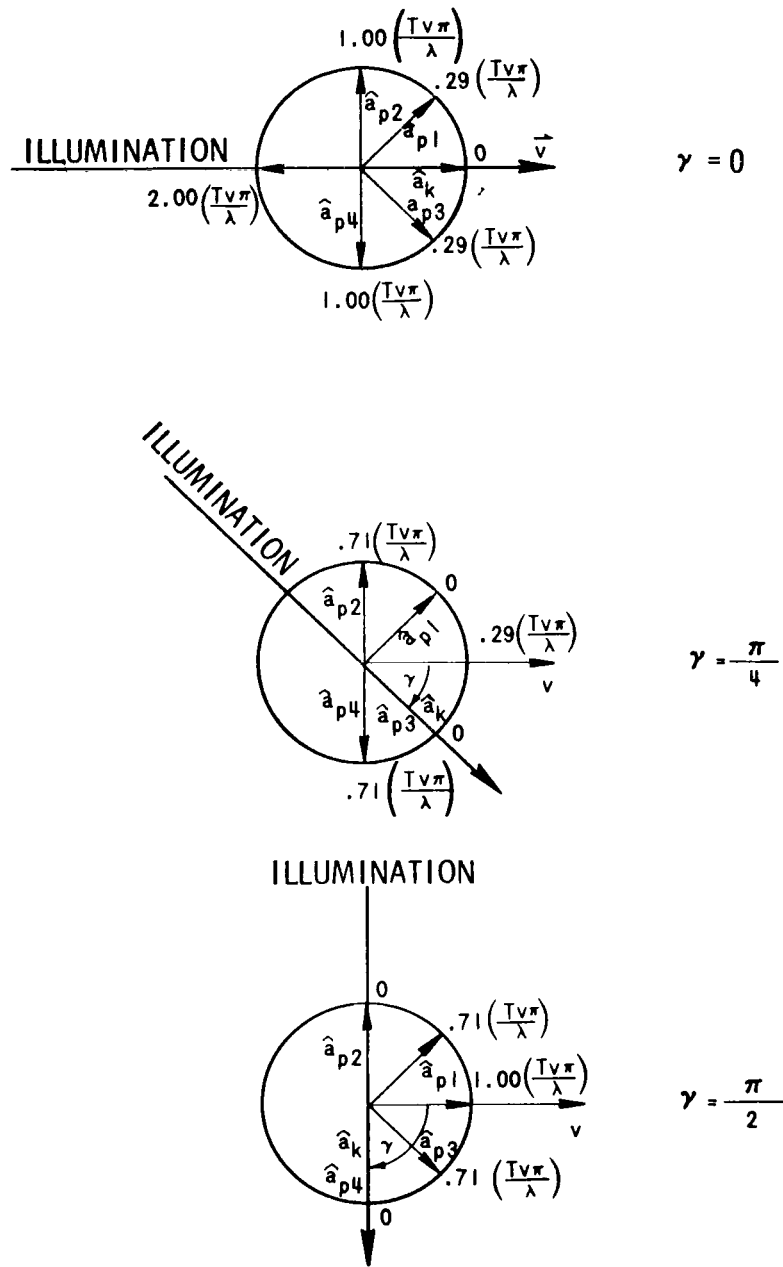
Figure 10. Variation of sinc-function argument with
illumination direction

Note the diagram in Figure 11 and let it be assumed that a hologram is to be formed in the x-y plane of this figure, which is a coordinate system with the origin at the center of the hologram. Analogous to the previous development, let

$$s = s' + S'' ,$$

where s' is the distance from the scene point, P(x, y), of the hologram and S'' is the distance from the laser source to the scene point, S. . (This is simply the total length of illumination called LQ + QP of the previous development.) Then, as before, because of of the motion of S, the rate at which S'' changes is:
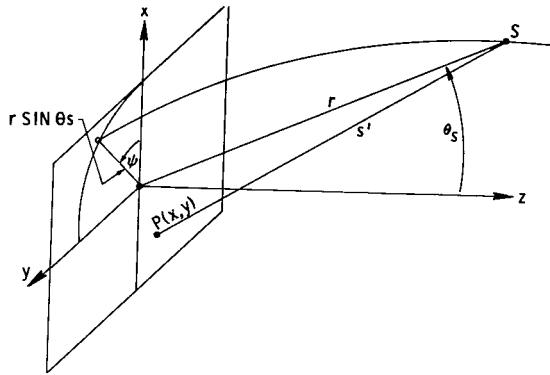
$$\frac{d(S'')}{dt} = \vec{V} \cdot \hat{a}_k = v \cos \gamma .$$

The coordinates for the point source which may be found from inspection of the previous diagram (Fig. 11) are given by:

Figure 11. Hologram-oriented coordinate system

$$x_s = r \sin \theta \cos \Psi ,$$

$$y_s = r \sin \theta \sin \Psi , \tag{49}$$

and

$$z_s = r \cos \theta .$$

Therefore, the distance, s', from the scene point, S, to a point, P(x, y), of the hologram is:

$$s' = \left[(x - x_s)^2 + (y - y_s)^2 + z_s^2 \right]^{\frac{1}{2}} , \tag{50}$$

20

which becomes

$$s' = r \left(\frac{x^2}{r^2} + \frac{y^2}{r^2} + 1 - \frac{2x}{r} \sin \theta \cos \Psi - \frac{2y}{r} \sin \theta \sin \Psi \right)^{\frac{1}{2}} .$$

By expanding, one obtains

$$s' = r \left(1 - \frac{x}{r} \sin \theta \cos \Psi - \frac{y}{r} \sin \theta \sin \Psi \right)$$

$$+ \frac{x^2}{2r^2} \left(1 - \sin^2 \theta \cos^2 \Psi \right) + \frac{y^2}{2r^2} \left(1 - \sin^2 \theta \sin^2 \Psi \right)$$

$$- \frac{xy}{r^2} \sin^2 \theta \sin \Psi \cos \Psi + \frac{x^3}{2r^2} \left(\sin \theta \cos \Psi - \sin^3 \theta \cos^3 \Psi \right)$$

$$+ \frac{x^2 y}{2r^2} \left(\sin \theta \sin \Psi - \sin^3 \theta \sin \Psi \cos^2 \Psi \right)$$

$$+ \frac{xy^2}{2r^3} \left(\sin \theta \cos \Psi - \sin^3 \theta \sin^2 \Psi \cos \Psi \right)$$

$$+ \frac{y^3}{2r^2} \left(\sin \theta \sin \Psi - \sin^3 \theta \sin^3 \Psi \right) + \text{(higher-order terms)} .$$

(51)

If one assumes that x/r and y/r are sufficiently small that only the first-order terms are needed, one obtains

$$s' = r \left(1 - \frac{x}{r} \sin \theta \cos \Psi - \frac{y}{r} \sin \theta \sin \Psi \right) .$$

(52)

To proceed, it becomes necessary to make some assumptions and then investigate some specific examples of the three orthogonal components of motion involved.

Following are derivations of the exposures for linear motions of a constant phase laser source, ϕ_s, along each of three orthogonal directions.

For a linear transverse motion (θ), consider the point source, S, to be moving with a constant radius, r_0, and in a constant Ψ plane, called Ψ_0,

such that

$$\theta = \theta_0 + \dot\theta t \qquad ;$$

then,

$$\sin \theta = \sin(\theta_0 + \dot\theta t)$$

and

$$\sin \theta = \sin \theta_0 \cos \dot\theta t + \cos \theta_0 \sin \dot\theta t \qquad .$$

However,

$$\sin \dot\theta t = \dot\theta t - \frac{(\dot\theta t)^3}{6} + \frac{(\dot\theta t)^5}{120} - \dots$$

and

$$\cos \dot\theta t = 1 - \frac{(\dot\theta t)^2}{2} + \frac{(\dot\theta t)^4}{24} - \dots \qquad .$$

If it is now assumed that $\dot\theta t$ is small enough that only the first term in each series need be used; then, one may write

$$\sin \theta = \sin \theta_0 + \dot\theta t \cos \theta_0 \qquad ;$$

then,

$$\sin^2 \theta = \sin^2 \theta_0 + 2 \dot\theta t \sin \theta_0 \cos \theta_0$$

and

$$\sin^3 \theta = \sin^3 \theta_0 + 3 \dot\theta t \sin^2 \theta_0 \cos \theta_0 \qquad .$$

If these conditions are now substituted into equation (51) for the distance, s', one obtains

$$s' = r_0 \left[1 - \frac{x}{r_0} (\sin \theta_0 + \dot{\theta} t \cos \theta_0) \cos \Psi_0 \right.$$

$$\left. - \frac{y}{r_0} (\sin \theta_0 + \dot{\theta} t \cos \theta_0) \sin \Psi_0 \right]$$

$$+ \frac{x^2}{2r_0^2} \left[1 - (\sin^2 \theta_0 + 2 \dot{\theta} t \sin \theta_0 \cos \theta_0) \cos^2 \Psi_0 \right]$$

$$+ \frac{y^2}{2r_0^2} \left[1 - (\sin^2 \theta_0 + 2 \dot{\theta} t \sin \theta_0 \cos \theta_0) \sin^2 \Psi_0 \right]$$

$$- \frac{xy}{r_0^2} \left[(\sin^2 \theta_0 + 2 \dot{\theta} t \sin \theta_0 \cos \theta_0) \sin \Psi_0 \cos \Psi_0 \right]$$

$$+ \frac{x^3}{2r_0^3} \left[(\sin \theta_0 + \dot{\theta} t \cos \theta_0) \cos \Psi_0 \right. \tag{53}$$

$$\left. - (\sin^3 \theta_0 + 3 \dot{\theta} t \sin^2 \theta_0 \cos \theta_0) \cos^3 \Psi_0 \right]$$

$$+ \frac{x^2 y}{2r_0^3} \left[(\sin \theta_0 + \dot{\theta} t \cos \theta_0) \sin \Psi_0 \right.$$

$$\left. - (\sin^3 \theta_0 + 3 \dot{\theta} t \sin^2 \theta_0 \cos \theta_0) \sin \Psi_0 \cos^2 \Psi_0 \right]$$

$$+ \frac{y^3}{2r_0^3} \left[(\sin \theta_0 + \dot{\theta} t \cos \theta_0) \sin \Psi_0 \right.$$

$$\left. - (\sin^3 \theta_0 + 3 \dot{\theta} t \sin^2 \theta_0 \cos \theta_0) \sin^3 \Psi_0 \right] + \text{(higher-order terms)}$$

Again, only the first-order terms are taken, equation (53) becomes

$$s' = r_0 \left[1 - \frac{x}{r_0} (\sin \theta_0 + \dot{\theta} t \cos \theta_0) \cos \Psi_0 \right.$$

$$\left. - \frac{y}{r_0} (\sin \theta_0 + \dot{\theta}_s t \cos \theta_0) \sin \Psi_0 \right] \quad ,$$

or

$$s' = r_0 - (x \cos \Psi_0 + y \sin \Psi_0) \sin \theta_0$$

$$- \dot{\theta} t (x \cos \Psi_0 + y \sin \Psi_0) \cos \theta_0 \quad .$$

Now, for simplicity, define

$$s_0' \equiv r_0 - (x \cos \Psi_0 + y \sin \Psi_0) \sin \theta_0 \quad ,$$

and one obtains

$$s' = s_0' - \dot{\theta} t (x \cos \Psi_0 + y \sin \Psi_0) \cos \theta_0 \quad . \tag{54}$$

Then, the rate of change of phase between S and P, because of the motion in the θ direction, is

$$\Omega_\theta = k \left(\frac{\partial s'}{\partial t} \right)_\theta = - k V_\theta \left[(x \cos \Psi_0 + y \sin \Psi_0) \frac{\cos \theta_0}{r} \right], \tag{55}$$

where

$$V_\theta = \dot{\theta} r \quad .$$

Proceeding in a similar fashion, the derivations for small motions in the r and Ψ directions may be obtained.

For linear radial motion, r , assume that the point source, S, moves with constant angles, θ_0 and Ψ_0 , such that

$$r = r_0 + \dot{r} t \quad ;$$

then,

$$\frac{1}{r} = \frac{1}{r_0 + \dot{r} t}$$

24

or

$$\frac{1}{r} = \frac{1}{r_0} \left[1 - \frac{\dot{r}t}{r_0} + \frac{(\dot{r}t)^2}{r_0^2} - \frac{(\dot{r}t)^3}{r_0^3} + \ldots \right] \quad ,$$

and for $\dot{r}t < r_0$,

$$\frac{1}{r^2} = \frac{1}{r_0^2} \left[1 - \frac{2\dot{r}t}{r_0} + \frac{3\,\dot{r}^2\,t^2}{r_0^2} - \ldots \right] \quad .$$

If the motion, $\dot{r}t$, is small compared with r_0, one may again neglect higher-order terms, and by using the above expressions in equation (51), s' becomes

$$s' = r_0 + \dot{r}t - x \sin \theta_0 \cos \Psi_0 - y \sin \theta_0 \sin \Psi_0$$

$$+ \left[\frac{x^2}{2r_0} (1 - \sin^2 \theta_0 \cos^2 \Psi_0) + \frac{y^2}{2r_0} (1 - \sin^2 \theta_0 \sin^2 \Psi_0) \right.$$

$$\left. - \frac{xy}{r_0} \sin^2 \theta_0 \sin \Psi_0 \cos \Psi_0 \right] \left(1 - \frac{\dot{r}t}{r_0} \right)$$

$$+ \left[\frac{x^3}{2r_0^2} (\sin \theta_0 \cos \Psi_0 - \sin^3 \theta_0 \cos^3 \Psi_0) \right.$$

$$+ \frac{x^2 y}{2r_0^2} (\sin \theta_0 \sin \Psi_0 - \sin^3 \theta_0 \sin \Psi_0 \cos^2 \Psi_0)$$

$$+ \frac{xy^2}{2r_0^2} (\sin \theta_0 \cos \Psi_0 - \sin^3 \theta_0 \sin^2 \Psi_0 \cos \Psi_0)$$

$$\left. + \frac{y^3}{2r_0^2} (\sin \theta_0 \sin \Psi_0 - \sin^3 \theta_0 \sin^3 \Psi_0) \right] \left(1 - \frac{2\dot{r}t}{r_0} \right) \quad .$$

Now, as before, taking only the first-order terms, one obtains

$$s' = r_0 + \dot{r}t - x \sin \theta_0 \cos \Psi_0 - y \sin \theta_0 \sin \Psi_0 \quad ,$$

and, considering the direction of k, one obtains the phase rate

$$\Omega_r = -k \left(\frac{\partial s'}{\partial t} \right)_r$$

$$\Omega_r = -k V_r \quad , \tag{56}$$

where

$$V_r = \dot{r} \quad .$$

For linear transverse motion, Ψ, the third orthogonal component, it is assumed that the point source, S, moves with constant radius, r_0, and angle, θ_0, such that

$$\Psi = \Psi_0 + \dot{\Psi} t \quad ;$$

then,

$$\sin \Psi = \sin \Psi_0 \cos \dot{\Psi} t + \cos \Psi_0 \sin \dot{\Psi} t$$

and

$$\cos \Psi = \cos \Psi_0 \cos \dot{\Psi} t - \sin \Psi_0 \sin \dot{\Psi} t \quad .$$

Further,

$$\sin \dot{\Psi} t = \dot{\Psi} t - \frac{(\dot{\Psi} t)^3}{6} + \frac{(\dot{\Psi} t)^5}{120} - \ldots$$

and

$$\cos \dot{\Psi} t = 1 - \frac{(\dot{\Psi} t)^2}{2} + \frac{(\dot{\Psi} t)^4}{24} - \ldots \quad .$$

Again, for small motion, $\dot{\Psi} t < \Psi_0$,

$$\sin \dot{\Psi} t \approx \dot{\Psi} t$$

and

$$\cos \dot{\Psi} t \approx 1 \quad .$$

Using the proper substitution of these relations in equation (51), one obtains the following for s':

$$
\begin{aligned}
s' = r_0 \Bigg\{ & 1 - \frac{x}{r_0} \sin \theta_0 \cos \Psi_0 - \frac{y}{r_0} \sin \theta_0 \sin \Psi_0 \\
& + \frac{x}{r_0} \sin \theta_0 \, \dot{\Psi} t \sin \Psi_0 - \frac{y}{r_0} \sin \theta_0 \, \dot{\Psi} t \cos \Psi_0 \\
& + \frac{x^2}{2r_0^2} (1 - \sin^2 \theta_0 \cos^2 \Psi_0) + \frac{x^2}{2r_0^2} \sin^2 \theta_0 \, \dot{\Psi} t \sin \Psi_0 \cos \Psi_0 \\
& + \frac{y^2}{2r_0^2} (1 - \sin^2 \theta_0 \sin^2 \Psi_0) - \frac{y^2}{r^2} \sin^2 \theta_0 \, \dot{\Psi} t \sin \Psi_0 \cos \Psi_0 \\
& - \frac{xy}{r_0^2} \sin^2 \theta_0 \sin \Psi_0 \cos \Psi_0 - \frac{xy}{r_0^2} \sin^2 \theta_0 \, \dot{\Psi} t \, (\cos^2 \Psi_0 - \sin^2 \Psi_0) \\
& + \frac{x^3}{2r_0^3} (\sin \theta_0 \cos \Psi_0 - \dot{\Psi} t \sin \theta_0 \sin \Psi_0 - \sin^3 \theta_0 \cos^3 \Psi_0 \\
& \qquad\qquad + 3 \dot{\Psi} t \sin^3 \Psi_0 \cos^2 \Psi_0) \\
& + \frac{x^2 y}{2r_0^3} [\sin \theta_0 \sin \Psi_0 \quad \dot{\Psi} t \sin \theta_0 \cos \Psi_0 \\
& \qquad - \sin^3 \theta_0 \sin \Psi_0 \cos^2 \Psi_0 + \dot{\Psi} t \sin^3 \theta_0 (2 \sin^2 \Psi_0 \cos \Psi_0 \\
& \qquad\qquad\qquad\qquad - \cos^3 \Psi_0)] \\
& + \frac{xy^2}{2r_0^3} [\sin \theta_0 \cos \Psi_0 - \dot{\Psi} t \sin \theta_0 \sin \Psi_0 \\
& \qquad - \sin^3 \theta_0 \sin^2 \Psi_0 \cos \Psi_0 - \dot{\Psi} t \sin^3 \theta_0 (2 \sin \Psi_0 \cos^2 \Psi_0 \\
& \qquad\qquad\qquad\qquad - \sin^3 \Psi_0)] \\
& + \frac{y^3}{2r_0^3} (\sin \theta_0 \sin \Psi_0 + \dot{\Psi} t \sin \theta_0 \cos \Psi_0 \\
& \qquad - \sin^3 \theta_0 \sin^3 \Psi_0 - 3 \dot{\Psi} t \sin^3 \theta_0 \sin^2 \Psi_0 \cos \Psi_0) \Bigg\} \quad .
\end{aligned}
$$

Again, taking only first-order terms, one obtains

$$s' = r_0 - x \sin \theta_0 \cos \Psi_0 - y \sin \theta \sin \Psi_0 + \sin \theta_0 \dot{\Psi} t \sin \Psi_0$$

$$- y \sin \theta_0 \dot{\Psi} t \cos \Psi_0 \quad ,$$

and again noting the direction of k,

$$\Omega_\Psi = - k V_\Psi \frac{(x \sin \Psi_0 - y \cos \Psi_0)}{r_0} \quad , \tag{57}$$

where

$$V_\Psi = \dot{\Psi} r_0 \sin \theta_0 \quad .$$

Any general linear motion may be resolved into the three orthogonal components used in the above development; i. e., (V_r, V_θ, V_Ψ). The constant portion will be a sum of the separate contributions to the phase shifts, and the time-variant portions will be formed by summing the time variant phases found for the three orthogonal components. The recorded fringe amplitude will then be modified by a sinc function whose argument is:

$$\frac{\Omega \tau}{2} = (\Omega_r + \Omega_\theta + \Omega_\Psi) \frac{\tau}{2} \quad .$$

Therefore, combining the time-variant and the constant portions of the phase shifts, the total phase retardation from the laser to the hologram by way of the scene is:

$$ks(t) = k \left[S_0'' + (\vec{V} \cdot \hat{a}_k) \tau \right] + k s_0' + (\Omega_r + \Omega_\theta + \Omega_\Psi) \tau$$

$$ks(t) = k [s_0' + S_0''] + (kv \cos \gamma + \Omega) \tau$$

$$ks(t) = k s_0 + (kv \cos \gamma + \Omega) \tau$$

where

$$\Omega = \Omega_r + \Omega_\theta + \Omega_\Psi \quad . \tag{58}$$

The exposure for this case of linear motion may be found by analogy with the exposure for the linear case represented by equation (26), where, by analogy, it can be seen that

$$kv \rightarrow kv \cos \gamma + \Omega \quad . \tag{59}$$

The exposure for this hologram–oriented coordinate case then becomes:

$$\mathscr{E}(P) = m\tau \left\{ K_c + E_r E_s \ \text{sinc} \left[\frac{k\tau}{2} (v \cos \gamma + \Omega) \right] \cos \phi \right\} \tag{60}$$

where the constants, m and K_c, are as defined earlier. Then the fringes are modulated by:

$$\text{sinc} \left[\frac{k\tau}{2} (v \cos \gamma + \Omega) \right] = \text{sinc} \frac{k\tau}{2} \left[v \cos \gamma \right.$$

$$- \frac{V_\theta}{r} (x \cos \Psi_0 + y \sin \Psi_0) \cos \theta_0$$

$$\left. - V_r - \frac{V_\Psi}{r} (x \sin \Psi_0 - y \cos \Psi_0) \right] .$$

$$\tag{61}$$

This is then the form of the cosine fringe modulation function in terms of the hologram–oriented coordinates.

If one lets $r \rightarrow \infty$, the sinc function of equation (61) becomes:

$$\text{sinc} \left[\frac{k\tau}{2} (v \cos \gamma + \Omega) \right]_\infty = \text{sinc} \left[\frac{k\tau}{2} (v \cos \gamma - V_r) \right] \quad . \tag{62}$$

Recall that δ is the angle between the velocity vector and a unit vector in the radial direction of the previous vector analysis development; then, by analogy,

$$V_r = \vec{V} \cdot \hat{a}_p = v \cos \delta \tag{63}$$

and equation (62) becomes

$$\text{sinc}\left[\frac{k\tau}{2}(v\cos\gamma + \Omega)\right]_{\infty} = \text{sinc}\left[\frac{k\tau v}{2}(\cos\gamma - \cos\delta)\right] \qquad (64)$$

and one has the identical result obtained in Section III.B.1.

C. The Resultant Effects of Linear Motion on the Reconstructed Wavefront

Section III.B compliments this subsection in showing that the effect of motion of a point source scene during the formation of a hologram is a modification of the recorded fringe contrast at various points of the hologram. Furthermore, it was stated that the effects on the hologram's recorded fringes caused by the scene motion may be derived by considering the motion of only a single point of a rigid moving scene.

Now the characteristics of the image reconstructed from a hologram having such motion-modified fringes will be investigated. Comparison of this image with the original object will give a point-spread function for the motion holography case. The approach which will be followed is that of the currently existing method presented in Reference 30.

Consider Figure 12, where a particular source distribution in the vicinity of the scene is assumed. It is desirable then to find the resulting amplitude and phase distribution on the hologram at the point, Q. If it can be shown that this is identical to the amplitude and phase distribution of the reconstructed field, it will prove that the assumed source will describe the reconstructed virtual image. One chooses a uniform line source lying along the motion vector as the assumed source (Fig. 12) i. e., the Z-axis in this diagram. The uniform line source of the length, $\Delta\ell$, is centered at the t = 0 scene point, s_0, and has a linear

Figure 12. Geometry for reconstruction analysis

30

phase variation, kbz, where b is some proportionality constant. The resulting field will be symmetrical with respect to revolution about the Z-axis. Then, it is desired to know the field at a point, Q, on the hologram, a distance, $q_0 >> \Delta \ell$, from the source, and at an angle, δ, from the Z-axis.

We consider that the field $\vec{dE}$ at the point, Q, is due to the contributions of point sources in the infinitesimal length, dZ, at a distance, Z, from the origin. Then, $\vec{dE}$ is given by:

$$\vec{dE} = \frac{A}{q_0} \exp \left[i(\omega t + kbZ - kq) \right] \, dZ \quad . \tag{65}$$

From the diagram,

$$q_0 = q + Z \cos \delta \quad ; \tag{66}$$

thus,

$$q = q_0 - Z \cos \delta \quad .$$

Then,

$$\vec{dE} = \frac{A}{q_0} \exp \left[i(\omega t + kbZ - kq_0 + kZ \cos \delta) \right] \, dZ \quad , \tag{67}$$

where A is a constant involving amplitude.

Now, by integrating, one finds the total field at Q:

$$\vec{E}(Q) = \frac{A}{q_0} \exp i(\omega t - kq_0) \int_{\Delta \ell/2}^{\Delta \ell/2} \exp \left[ik(b - \cos \delta) Z \right] dZ \quad . \tag{68}$$

Applying Euler's formula to the integral and setting in the limits of integration,

$$\vec{E}(Q) = \frac{A}{q_0} \exp i(\omega t - kq_0) \left\{ \frac{2 \sin \left[k(b - \cos \delta) \Delta \ell/2 \right]}{k(b - \cos \delta)} \right\} \quad . \tag{69}$$

Upon multiplying the brackets by $\Delta \ell / \Delta \ell = 1$, one finds that

$$\vec{E}(Q) = \frac{A}{q_0} \exp i(\omega t - kq_0) \Delta \ell \, \text{sinc} \left[k(b - \cos \delta) \Delta \ell/2 \right] \quad . \tag{70}$$

31

Therefore, $E(Q)$ represents a homocentric wave, centered at the origin point, 0, with an amplitude weighting given by:

$$\text{sinc} \left[\frac{k \Delta \ell}{2} (b - \cos \delta) \right] \quad . \tag{71}$$

Equation (70) is the description of the field at the point, Q, of the hologram plane resulting from the assumed source of a uniform line.

It is now appropriate to determine the amplitude and phase distribution of the hologram's reconstructed field and then compare the reconstructed (virtual image) field with that of the assumed source. If the two are identical, it will be obvious that the assumed source will describe the reconstructed virtual image.

For the reconstructed hologram, the amplitude transmission factor may be writtin (see the Appendix) as:

$$T_a = T_0 - k_f \, \mathscr{E} \, . \tag{72a}$$

The exposure, $\mathscr{E}$, is given by equation (37),

$$\mathscr{E} = m\tau \left\{ K_c + E_r E_s \, \text{sinc} \left[\frac{k\tau \vec{V}}{2} \cdot (\hat{a}_k - \hat{a}_p) \right] \cos (\phi_r - \phi_s) \right\} ,$$

or

$$\mathscr{E} = K_1 + K_2 \, \text{sinc} \left[\frac{k\tau \vec{V}}{2} \cdot (\hat{a}_k - \hat{a}_p) \right] \cos (\phi_r - \phi_s) \quad . \tag{72b}$$

Then, from the amplitude transmission factor, one can write:

$$T_a = T_0 - k_f \left\{ K_1 + K_2 \, \text{sinc} \left[\frac{k\tau \vec{V}}{2} \cdot (\hat{a}_k - \hat{a}_p) \cos (\phi_r - \phi_s) \right] \right\}$$

or

$$T_a = T_0 - K_1' + K_2' \, \text{sinc} \left[\frac{k\tau \vec{V}}{2} \cdot (\hat{a}_k - \hat{a}_p) \cos (\phi_r - \phi_s) \right] \quad . \tag{73}$$

Now, since equations (72) and (73) describe the exposure and development of the field resulting from a motion scene, the reconstructed virtual image field (first-order diffraction) has an amplitude proportional to the magnitude of the spatial variations in the amplitude transmission factor and is, therefore, proportional to:

32

$$\text{sinc}\left[\frac{k\tau\vec{V}}{2} \cdot (\hat{a}_k - \hat{a}_p)\right] = \text{sinc}\left[\frac{kv\tau}{2}(\cos\gamma - \cos\delta)\right]. \tag{74}$$

Therefore, since the fringe phase, $(\Phi_r - \Phi_s)$, is independent of the motion, $\vec{V}$, the hologram will reconstruct a homocentric wave with the center at the $t = 0$ position of the scene point.

Then, comparing equations (71) and (74), one sees that, if $\Delta\ell = v\tau$ and $b = \cos\gamma$, the phase fronts and amplitude distributions are identical for the assumed source and the reconstructed (virtual image) field of the hologram. Therefore, the virtual image will be a line source of length, $v\tau$, and with a phase equal to $KZ\cos\gamma$, where Z is the distance from the center of the source. In other words, the image will have the same blur as results from any detector (such as a conventional photograph) having an integrating time of τ. Furthermore, the phase relationships between the impluses that sequentially formed the hologram are preserved.

IV. ANALYTICAL AND EXPERIMENTAL RESULTS

A. A Unique Holographic Technique That Allows Resolution of Front-Surface Detail From Scenes Moving Linearly at High Velocities

Front-surface resolution from targets moving with a velocity of the order of 9×10^5 cm/s will be obtainable if one uses a specific orientation of the holographic system [31]. With the specific orientation described below, the path length of the reflection arm is constrained to change by an amount equal to $\lambda/8$ and, thereby, should allow front-surface resolution heretofore unobtainable for moving targets by conventional methods. (The choice of $\lambda/8$ was arbitrary, and simply satisfied the need to be smaller than $\lambda/2$.)

The specific orientation of a holographic system referred to above also involves the use of a hypothetical ellipse oriented with its major axis parallel to the line of motion defined by the moving projectile.[1] This line of

---

1. In this section, a projectile target is discussed, although the actual target tested was a rotating disc whose tangential velocity approximated linear motion (Section IV.D.1). The concept of projectile target or scene facilitates the understanding of this section.

motion must be made tangent to the hypothetical ellipse at a certain point, Q. One possible configuration of a holographic system[2] positioned in this preferred orientation, inside the hypothetical ellipse, is shown in Figure 13. The specific orientation is defined by the following conditions: (1) a thin-film beam-splitter (b/s) centered at the focus, f_2, of the hypothetical ellipse, and (2) a film plane centered at the other focus, f_2, and the major axis of this ellipse, defined by XX' in Figure 13, being parallel to the tangent line, PP', of Figure 13, which may be identified as the line of motion of the high-speed projectile referred to above; similarly, it may be defined as a tangent to the rim of a spinning wheel whose tangential velocity may be very high. More generally, PP' may be defined as a line coincident with the linear velocity vector of the moving scene under investigation.

The system may be described as follows (Fig. 13): Laser radiation is incident on the first thin-film beam splitter (b/s), centered at the focus, f_1. The transmitted beam from here is made incident on the projectile that is moving along the tangent line, PP', and is momentarily at the point, Q, on the perpendicular bisector of XX'. The beam is then reflected from the projectile and made incident on the film,

Figure 13. Hybrid holography system with an elliptic orientation

centered at the focus, f_2. The reflected beam, from the beam-splitter at f_1, is made incident on a second beam-splitter (b/s), just slightly displaced from f_1, where it is again split into two beams. This transmitted beam constitutes the reference beam for the system and after a reflection from a mirror, M (Fig. 13), this reference beam is made incident on the film at focus, f_2. The reflected beam from the last beam-splitter is used as a second signal beam that backlights the target via a diffuser plate (Fig. 13). After being incident on a mirror, M_2, this signal beam passes through a diffuser plate in the region of the projectile, where it then is incident on the film at focus, f_2, after being reflected by another mirror, M_3.

From the use of the backlighting arm, at least one is reasonably assured of a backlighted hologram; i. e., a silhouette of the moving projectile. (See holographic type 3, Section II.) With this information, one has more

---

2. This specific system is termed a hybrid system [25] and has been patented by the U. S. Government for its inherent advantages for holography of moving targets.

freedom to manipulate the hypothetical ellipse until the front-surface resolution of the silhouetted projectile is obtained.

The exact matching of the length of the three arms is of no real concern if one has a source with sufficient coherence length. The source being used in this experiment has a coherent length greater than 3 m, operates at the 0.6943 μm ruby line and has a pulse length as short as 25 nsec.

Figure 14a shows that the general equations of such an ellipse are given by:

$$b^2 x^2 + a^2 y^2 = a^2 b^2 \qquad . \tag{75}$$

The line segment, PP', is considered to be tangent to this ellipse at the point Q, which lies on the perpendicular bisector of XX'. The segment line, PP', in Figure 14a is identical to the tangent line, PP', of Figure 13. It is the line of motion of the high-speed projectile, and is parallel to the major axis, XX', of the ellipse and may be considered perfectly straight. The projectile travels along PP' (Fig. 14a) and reaches Q at t_0. The radiation incident at t_0 will be reflected to the film, which is positioned at f_2. At this particular moment, the hypothetical ellipse passes through Q, with a beam-splitter at f_1 and a film at f_2, and creates the situation depicted earlier in Figure 13.

As the projectile moves some incremental distance, Δx, along PP' and past Q, it moves off this initial ellipse, but it can be considered to move immediately onto another ellipse, just slightly larger than the initial one. If the elliptic constant of the initial ellipse was 2a, the elliptic constant of this new ellipse will be $2(a + \Delta a)$. The radiation reflected from this moving projectile will then be incident on the film at f_2 and will interfere there with the reference beam as long as $2\Delta a$ is less than $\lambda/2$.

Figure 14b shows that a family of such ellipses is constructed, each successive ellipse being intercepted by PP' as one moves from Q to the right along PP' parallel to the x-axis of the coordinate system. It is clear that the separation of the foci remains constant and equal to 2d for the entire family of curves. Figure 14c is a convenient enlargement of the first quadrant of Figure 14b. The points of interception of PP' with each successive member of the family of ellipses are given by P_1, P_2, P_3, etc., respectively. It is

maintained that, as PP is traveled to the right, the original ellipse can be considered to grow successively to the next larger member of its family, while 2d remains constant.

If the ellipse is considered to be enlarged during t, then by expanding to a larger ellipse, equation (75) becomes:

$$b^2 x \Delta x + b \Delta b x^2 + a^2 y \Delta y + a \Delta a y^2 = a^2 b \Delta b + b^2 a \Delta a \qquad . \qquad (76)$$
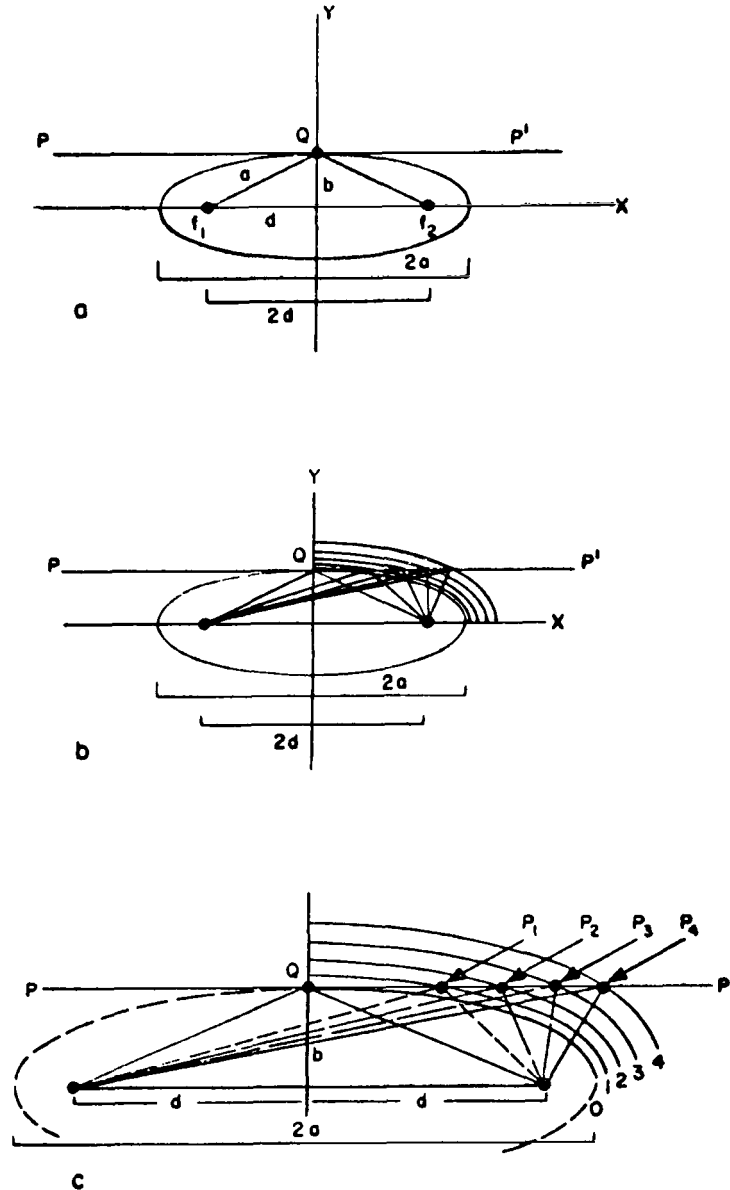
Figure 14. Family of successive ellipses with constant separation of foci 2d

36

Since the direction of projectile motion is parallel to the x-axis, $\Delta y \equiv 0$ and

$$b^2 x \Delta x = a \Delta a \ (b^2 - y^2) + b \Delta b \ (a^2 - x^2) \quad . \tag{77}$$

However, from Figure 14a,

$$a^2 - b^2 = d^2 \quad , \tag{78}$$

where d is a constant; therefore,

$$a \Delta a = b \Delta b \tag{79}$$

and equation (77) becomes:

$$b^2 x \Delta x = a \Delta a \ [a^2 + b^2 - (x^2 + y^2)] \quad . \tag{80}$$

From the basic equation for our ellipse, equation (75), one easily obtains:

$$x^2 + y^2 = b^2 + x^2 \ [1 - (b^2/a^2)] \quad . \tag{81}$$

Upon substituting equation (81) into equation (80), one has

$$x \Delta x = (\Delta a / ab^2) \ (a^4 - d^2 x^2) \quad . \tag{82}$$

For any ellipse, $2a = L$, where L is a constant and at present is the optical path length of the front illumination signal arm. When the ellipse expands because of projectile travel along $\overline{PP}'$, $2a = L$ becomes $2 \Delta a = \Delta L$. Therefore, since $\Delta a = \Delta L/2$, equation (82) becomes:

$$x \Delta x = (\Delta L/2) \ (1/ab^2) \ (a^4 - d^2 x^2) \quad . \tag{83}$$

Q has been taken as the reference point for x (i.e., x is zero when the projectile is at Q); therefore, as measurement of the projectile motion starts from Q and traverses to some P, $x = \Delta x$ and equation (83) becomes

$$(\Delta x)^2 = \left(\frac{\Delta L}{2}\right) \left(\frac{1}{ab^2}\right) [a^4 - d^2 \ (\Delta x)^2] \tag{84}$$

37

or

$$(\Delta x)^2 = \frac{\Delta L\, a^3/2\, b^2}{1 + \dfrac{\Delta L\, d^2}{2\, a\, b^2}} \qquad . \tag{85}$$

Making the assumption that d^2 is not drastically different from b^2 and $\Delta L/2 << a$, one has:

$$\frac{\Delta L\, d^2}{2\, a\, b^2} << 1 \qquad ,$$

and equation (85) becomes:

$$(\Delta x)^2 \approx \left(\frac{\Delta L}{2}\right)\left(\frac{a^3}{b^2}\right) \qquad , \tag{86}$$

where $\Delta L = 2\,\Delta a$ is the variation in the original elliptic constant $2a$ caused by the travel, Δx, of the projectile along $\overline{PP}{}'$. At a given velocity, v, for τ,

$$\Delta x = v\tau , \tag{87}$$

where τ is the pulse length of the laser and thereby the exposure time.

Equation (86) is, therefore, an expression that relates the distance, Δx, traveled by the projectile along $\overline{PP}{}'$, to the total change in elliptic constant, $\Delta L = 2\,\Delta a$; i. e., ΔL is the change in optical length of the front-surface illumination arm of the holographic system. Substituting equation (87) into equation (86) and solving for the projectile velocity yields:

$$v = \left(\frac{\Delta L}{2}\right)^{\frac{1}{2}} \frac{a^{\frac{3}{2}}}{b\,\tau} \qquad . \tag{88}$$

This relation may be used to determine the permissible projectile velocities allowed by the specfic configuration having a set of elliptic parameters and a specified tolerance, ΔL. For illustration, one arbitrarily sets ΔL equal to $\lambda/8$ ($\lambda = 6943\ \text{Å}$) and lets the distance of separation between the center of the first beam-splitter at f_1 and the center of the photographic film at f_2 be a constant value, $2d$. By varying the semimajor axis, a, which in turn varies the

semiminor axis, b, one may obtain a set of allowed distances of travel, $\Delta x = v\tau$. This set of Δx values is graphically shown in Figure 15, where one has used the allowed Δx values as ordinate and the arbitrarily chosen values of semimajor axis, a, as abscissa. Each separate curve corresponds to a specific value of d and the elliptic parameters are related by $a^2 = d^2 + b^2$.
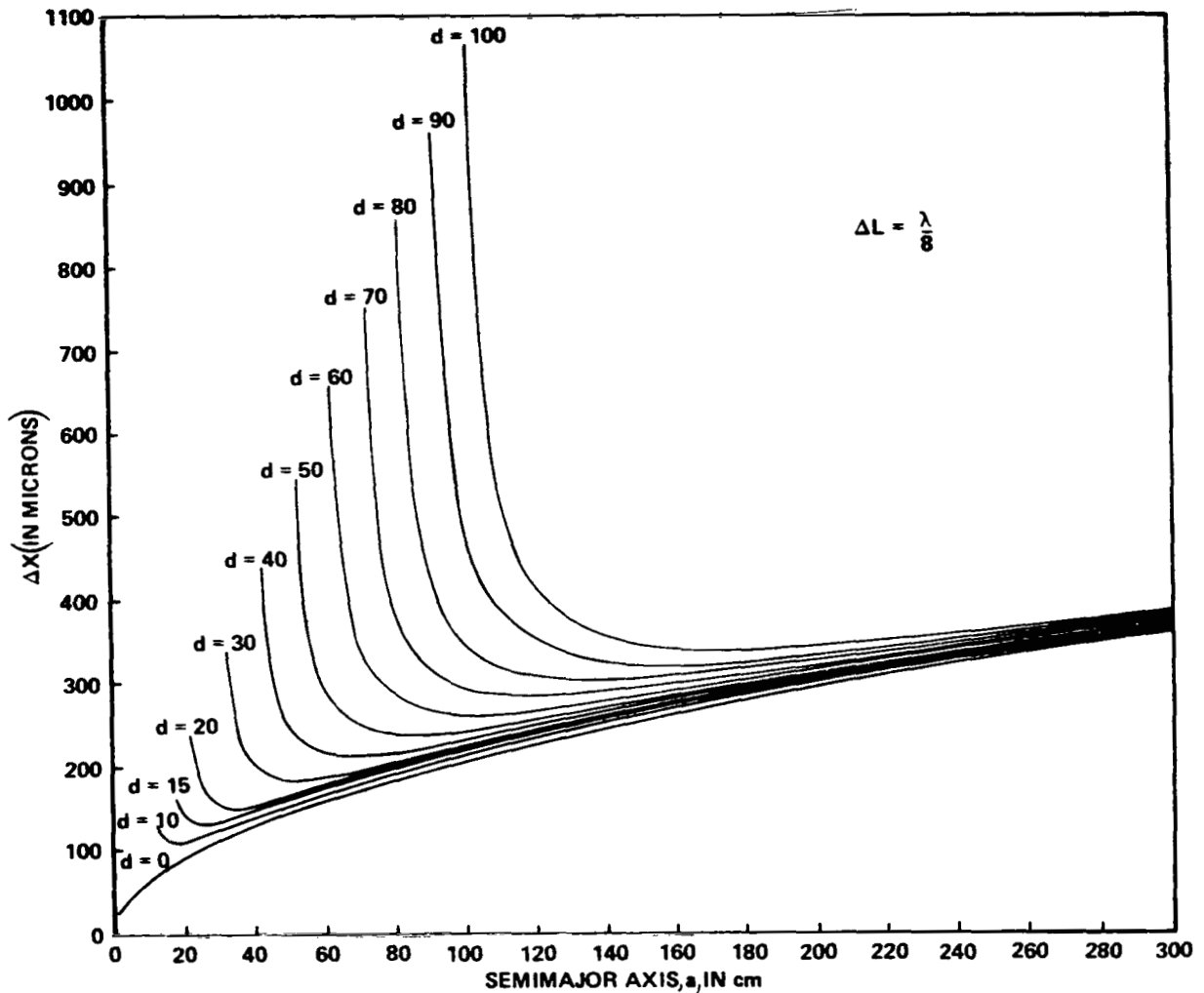

Figure 15. Allowed travel, ΔX, for various elliptical configurations

It may be interesting to note the following:

1. For this fixed value of $\Delta L = \lambda/8$ and each assigned value of d, the curve approached the vertical line, $a = d$, asymptotically. This seems to indicate that the projectile velocity can be any high value without limit if $a = d$.

Obviously, this is not practical since at a = d, b ≡ 0, and the projectile would have to pass directly through the beam-splitter and film. However, picking the smallest practical value of b allows the highest possible velocity for a given value of d. As the assigned value of d increases (bounded by some practical value of d), the curve rises and thereby raises the allowed value of velocity, although, because of the steepness of the curve, this region (of the asymptotic limit for a given curve where a > d) may be unstable with respect to changes in a or b.

2. As the assigned value of d decreases, the respective curve lowers. The lower bound for these curves occurs at d = 0; the hypothetical ellipse becomes a circle. This is again impractical since the beam-splitter would be located at the photographic plate.

3. Differentiation of equation (88) shows that each curve has a minimum at the value of $a = \sqrt{3}\, d$. Substitution of this result back into equation (88) produces

$$v_{min} = \frac{3^{\frac{3}{4}}}{2} \left(d\, \frac{\Delta L}{\tau^2} \right)^{\frac{1}{2}} \qquad . \qquad (89)$$

The minimum permissible value of the velocity, v_{min}, is that which falls on the curve for each specific value of d. (Obviously, all values of velocity lower than v_{min} are still permissible since lower velocities will cause even less shift in the path length than the arbitrarily chosen $\lambda/8$.) Because each curve has a zero slope at this point, the region about this point is the most stable (i. e., for a given curve value of d) with regard to possible changes in the value of the elliptical parameters a or b. Therefore, changes in b and a might occur because of the projectile varying slightly off the path as it travels along the line of motion.

The system description above has been for a moving point only; however, the contribution of a point in the rigid moving scene to the total reconstructed wave is independent of other points in the scene; i. e., the principle of super-position applies to the holography of moving rigid scenes.

B. Application of the Theory of Motion Holography to the Holographic Technique Under Investigation

Two theoretical approaches to the motion holography problem were developed in Section III.C. Both approaches were equivalent to first order. For application here, the scene-oriented coordinate approach shall be used, since it allows more physical insight into the problem.

40

Figure 16 should be considered which represents a typical elliptical configuration such as that investigated in Section IV.A and subsequently tested experimentally.
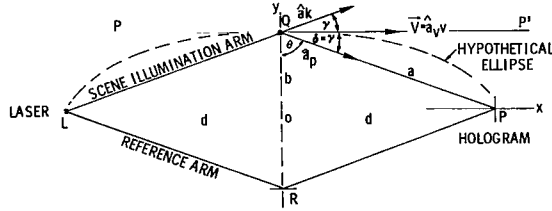
Figure 16. Typical elliptical configuration

Consider a single point of the scene, Q having a linear velocity, $\vec{V}$, parallel to the x-axis. As before, consider the point, R, on the reference arm as our reference point. Let L be a point on some reference phase front from the laser, which is common to both beams, because of the presence of a beam-splitter. Let Q represent a single point of the scene having the coordinates (o, b); i. e., lying on the y-axis. Let $\hat{a}_p$ be a unit vector along the line from the scene point, Q, to the hologram point, P. Let $\hat{a}_k$ be a unit vector along the direction of propagation of the incident laser radiation at the scene point. Let $\hat{a}_v$ be a unit vector indicating the velocity of point Q. Then the angle γ between $\hat{a}_k$ and $\hat{a}_v$ is equal to the angle δ between $\hat{a}_p$ and $\hat{a}_v$.

It is assumed that the reference beam is constant in its length. The scene illumination beam is composed of two parts: LQ + QP. The rate of change of the partial path length, LQ, from the laser to the scene point, Q, is:

$$\vec{V} \cdot \hat{a}_k = v \cos \gamma \quad . \tag{90}$$

The rate of change of the path length, QP, from the scene point, Q, the hologram point, P, is given by:

$$\vec{V} \cdot \hat{a}_p = v \cos \delta = v \cos \gamma \quad . \tag{91}$$

Following, identically, the procedure of Section IV.C., one finds the expression for the exposure, because of the motion of this point, from equation (37); i. e.,

$$\mathcal{E}(P) = m\tau \left\{ K_c + E_r E_s \, \text{sinc} \left[\frac{kv\tau}{2} (\cos \gamma - \cos \delta) \right] \cos \Phi \right\} , \tag{92}$$

where $K_c = E_r^2 + E_s^2$ is constant, $\Phi = k(s_0 - r)$ is the time-invariant portion of the phase, and m is the constant because of the intensity defined earlier.

Using equation (91),

$$\mathcal{E}(P) = m\tau \left\{ K_c + E_r E_s \text{ sinc} \left[\frac{kv\tau}{2} (\cos \gamma - \cos \gamma) \right] \cos \Phi \right\} . \qquad (93)$$

Therefore, the sinc function for the scene point at Q is

$$\text{sinc} \left[\frac{kv\tau}{2} \right] (0) = \text{sinc } (0) = 1 . \qquad (94)$$

Then it can be seen that the reconstruction of Q will be a maximum. It will still be a bright reconstruction as long as its travel along $\hat{a}_v$ is some small quantity $\Delta x < < QP$; in other words, as long as Δx of Q is small enough that $\delta \approx \gamma$.

Figure 17. Plot of sinc $x = \dfrac{\sin x}{x}$
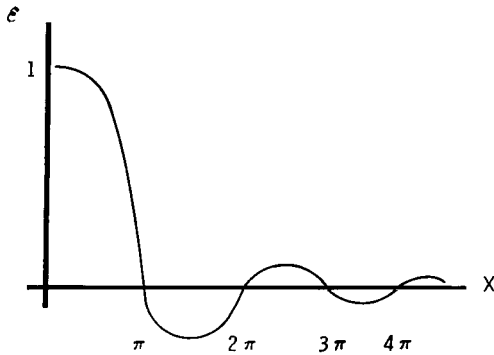
To place some value on the allowed magnitude of Δx, such that $\delta \approx \gamma$, attention is directed to a plot of the sinc function (Fig. 17). It can be seen that, if the total path length,

$$S = LQ + QP ,$$

is restricted to change by an amount $\leq \lambda/2$ (where this change is caused by total motion Δx), a hologram is obtained. If this change is further restricted to $\lambda/8$, a reasonably bright hologram will result.

In Section IV.A an expression was derived for the total allowed scene travel, Δx, along the direction of $\hat{a}_v$ in terms of the parameters of an ellipse and quantity, ΔL, which was the total change in path length, S. The following expression is from equation (86):

$$v = \left(\frac{\Delta L}{2} \right)^{\frac{1}{2}} \frac{a^{\frac{3}{2}}}{b\tau}$$

and, from equation (87) it becomes

$$\Delta x = \left(\frac{\Delta L}{2}\right)^{\frac{1}{2}} \frac{a^{\frac{3}{2}}}{b} \qquad . \tag{95}$$

The magnitude of Δx, sufficient to cause a change in total path length, S, of $\lambda/8$ and $\lambda/2$, has been tabulated in Table 1 for various ellipses and a wavelength λ, equal to 0.6943μm.

If one chooses $\Delta L = \lambda/8$, then

$$\Delta x \quad \left(\frac{\lambda}{16}\right)^{\frac{1}{2}} \frac{a^{\frac{3}{2}}}{b} \qquad , \tag{96}$$

and, since

$$\Delta x = v\tau \tag{97}$$

is the total allowed travel of the scene during exposure; then, from equation (92), the expression for the scene exposure for the elliptical configuration is:

$$\mathscr{E}(P) = m\tau \left\{ K_c + E_r E_s \ \text{sinc} \left[\frac{k\Delta x}{2} (\cos \gamma - \cos \delta) \right] \cos \Phi \right\}. \tag{98}$$

Specifically, the sinc function for this symmetrical scene point, Q, is, upon substitution of equation (96),

$$\text{sinc} \left[\frac{k \lambda^{\frac{1}{2}} a^{\frac{3}{2}}}{8b} (\cos \gamma - \cos \delta) \right] \qquad , \tag{99}$$

where, for this point, Q,

$$\delta \approx \gamma \quad .$$

C. Comparison of Vector Analysis Approach to the Description in Terms of Elliptic Parameters

A discussion will now ensue which is intended to provide an intuitive understanding concerning the motion holography problem. Again, the approach is based on the vector analysis of Section III and, therefore, considers only

TABLE 1. Δx FOR SYSTEMS INVESTIGATED

d (cm)	Semi-Major Axis = a (cm)	Semi-Minor Axis = b (cm)	$\Delta x \frac{\lambda}{8}$ (μ)	$\Delta x \frac{\lambda}{2}$ (μ)
15	18	9.95	159.88	319.79
	20	13.23	140.84	281.69
	22	16.09	133.57	267.13
	24	18.74	130.73	261.46
	25.5 (Min:a $=\sqrt{3d}$)	20.50	128.50	257.00
	26	21.24	130.04	260.09
	50	47.70	154.41	308.82
	100	98.87	210.70	421.34
	200	199.44	295.43	590.86
	300	299.63	361.26	722.52
20	22	9.17	234.54	469.07
	24	13.27	184.62	369.24
	26	16.61	166.23	332.47
	30	22.34	153.08	306.15
	34 (Min:a $=\sqrt{3d}$)	27.50	150.20	300.40
	40	34.64	152.13	304.26
	50	45.83	160.72	321.23
	100	97.98	212.61	425.21
	200	199.00	296.08	592.16
	300	299.33	361.61	723.22
30	32	11.14	338.63	677.27
	36	19.90	226.11	452.22
	40	26.46	199.18	398.37
	48	37.47	184.88	369.76
	51 (Min:a $=\sqrt{3d}$)	41.00	182.00	364.00
	70	63.25	192.90	385.80
	100	95.40	218.37	436.74
	150	146.97	260.39	520.78
	200	197.74	297.97	595.94
	300	298.50	362.62	725.25
50	52	14.28	546.89	1093.79
	60	33.17	291.91	583.81
	70	48.99	249.03	498.06
	80	62.45	238.68	477.36
	85 (Min:a $=\sqrt{3d}$)	69.00	235.72	471.44
	90	74.83	237.68	475.35
	96	81.95	239.09	478.18
	100	86.60	240.54	481.08
	200	193.65	304.26	608.52·
	300	295.80	365.92	731.85

44

first-order effects. It is further based on the results of the use of the elliptical configuration holographic technique of Section IV.A. The resulting facts will prove most useful for the experimentalist, whether he desires to minimize the effect of motion (resolution of front-surface detail) or to maximize the effects of motion (vibration analysis).

Figure 18. Diagram for $\vec{V}_{||}$ computation

Figure 18 shows that all the parameters have the definitions given previously.

Assume that the scene moves with a velocity, $\vec{V}$, which is referenced to the bisector line, OQ (the y-axis). Then,

$$\vec{V} = \vec{V}_{||} + \vec{V}_{\perp} \quad , \qquad (100)$$

where $\vec{V}_{||}$ is the velocity component parallel to the bisector, OQ, and $\vec{V}_{\perp}$ is the velocity component perpendicular to OQ.

As before, let the total path length from the laser to the hologram point, P, be given by:

$$S = LQ + QP \quad .$$

Then, the rate of change of the total path length is:

$$\frac{dS}{dt} = \vec{V} \cdot (\hat{a}_k - \hat{a}_p)$$

or

$$\frac{dS}{dt} = \left(\vec{V}_{||} + \vec{V}_{\perp} \right) \cdot (\hat{a}_k - \hat{a}_p) \quad . \qquad (101)$$

However, since $(\hat{a}_k - \hat{a}_p)$ lies along the bisector, OQ, and since $\vec{V}_{\perp}$

is normal to OQ, $\cos \pi/2 = 0$ and

$$\vec{V}_\perp \cdot (\hat{a}_k - \hat{a}_p) = 0 \qquad .$$

Therefore,

$$\frac{dS}{dt} = \vec{V}_{||} \cdot (\hat{a}_k - \hat{a}_p) \tag{102}$$

and only motion along the bisector, OQ (i. e., the y-axis for the elliptical configuration), contributes to hologram degradation (first order).

For general linear motion (not necessarily parallel to the x-axis of our ellipse), the modifying function in equation (92) may be written as

$$\operatorname{sinc}\left[\frac{k\tau \vec{V}}{2} \cdot (\hat{a}_k - \hat{a}_p) \right] = \operatorname{sinc}\left[\frac{k\tau}{2}\left(\vec{V}_{||} + \vec{V}_\perp \right) \cdot (\hat{a}_k - \hat{a}_k) \right]$$

$$= \operatorname{sinc}\left\{ \frac{k\tau}{2}\left[\vec{V}_{||} \cdot (\hat{a}_k - \hat{a}_p) + \vec{V}_\perp \cdot (\hat{a}_k - \hat{a}_p) \right] \right\}$$

$$= \operatorname{sinc}\left\{ \frac{k\tau}{2}\left(\left|\vec{V}_{||}\right| \left|\hat{a}_k\right| \cos\theta \right. \right.$$

$$\left. \left. + \left|\vec{V}_{||}\right| \left|-\hat{a}_p\right| \cos\theta \right) \right\}$$

$$= \operatorname{sinc}\left(\frac{k\tau}{2} v_{||} \, 2 \cos\theta \right)$$

$$\operatorname{sinc}\left[\frac{k\tau \vec{V}}{2} \cdot (a_k - a_p) \right] = \operatorname{sinc}\left(k\tau v_{||} \cos\theta \right) \qquad . \tag{103}$$

An appeal is made again to the plot of the sinc function given in Figure 17. One can see that a good (bright reconstruction) hologram may be obtained if the argument of the sinc function is kept $\leq \pi/2$ (this means an allowed change in the total path length, S, of $\lambda/4$).

Then, from equation (103), one writes

$$k\tau v_{||} \cos\theta \leq \pi/2 \qquad .$$

Since $k = \dfrac{2\pi}{\lambda}$ one then has

$$\Delta y = \tau v_{||} \leq \frac{\lambda}{4 \cos \theta} \quad , \qquad\qquad (104)$$

where θ is the half angle shown in Figure 18.

Therefore, the total allowed motion along the y direction (i. e., in the direction of $\vec{V}_{||}$) must be less than or equal to $\dfrac{\lambda}{4 \cos \theta}$.

In Section IV.A, the allowed motion of the typical elliptical system was described but in an entirely different language, that of the parameters of an ellipse. The value of d was considered to be constant, where d is the distance of separation of each foci from the origin. Now, for any ellipse,

$$a^2 = b^2 + d^2 \quad , \qquad\qquad (105)$$

one may write

$$\Delta b = \frac{a}{b} \, \Delta a \quad . \qquad\qquad (106)$$

From the diagram of Figure 18, one may make the observation that Δb is just the total allowed motion along the y direction; then,

$$\Delta b = \Delta y = v_{||} \, \tau \qquad\qquad .$$

Now, combining the last two equations and observing that $a/b = \sec \theta$

$$\Delta y = \Delta a \, \theta \quad . \qquad\qquad (107)$$

Since Δa is just that change in the total path length, S, caused by motion, Δy, along the y direction, which will allow a bright reconstruction of the hologram, one uses $\Delta a \leq \lambda/4$ and equation (107) to obtain

$$\Delta y \leq \frac{\lambda}{4} \, \sec \theta \qquad\qquad (108)$$

or

$$v_{||} \tau \leq \frac{\lambda}{4 \cos \theta} \qquad\qquad \bullet \qquad\qquad (109)$$

47

A comparison of equations (104) and (109) shows the necessary agreement between the description in terms of elliptic parameters and that of scene-oriented coordinates. This expression will be of considerable interest in the next section.

One observes that for a silhouette hologram (backlighted, diffuse or direct type), $\theta = \pi/2$ and any motion is acceptable. If the direction of motion is known and the resolution of front-surface detail is desired, the elliptic configuration investigated is highly desirable since here the hologram is placed such that the bisector, OQ, is normal to the velocity vector. This makes $v_{||} = 0$ and maximizes the hologram quality. This is strictly true, of course, only for straight-line motion of v.

D. Experimental Results of the Elliptical Configuration

In the following paragraphs the systems tested are identified.

1. <u>System Identification and Description</u>. During the experimental investigation of the elliptical configuration technique, many elliptical configurations were tested. In each case, the linear target velocity along the x direction was approximated by the tangential rim velocity of a wheel of radius, r, centered at the symmetrical point, (o, b), of the respective elliptical configuration. The reason for this choice and the degree of approximation will be presented later.

Figure 19. General configuration

Of the systems tested, five different configurations were selected that will now be described. Figure 19 diagramatically describes a general configuration. Radiation from the ruby laser, $\lambda = 0.6943 \ \mu m$, is made incident of beamsplitter, BS, at foci, f_1, by the mirror, M_1. Here, the beam is split into two beams: the object wave and the reference wave. The object wave is incident on the rim of the ta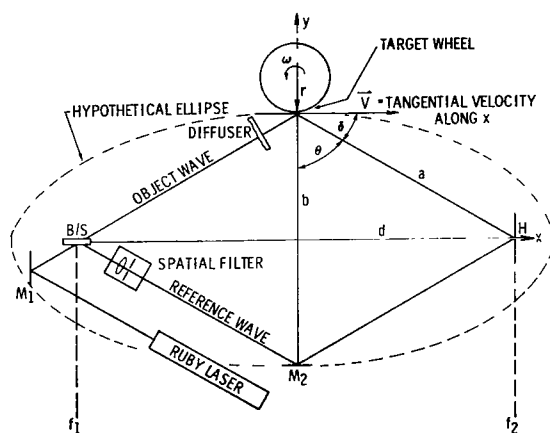rget wheel of radius, r, after passing through the diffuser. Radiation that was scattered by the edge of the wheel is made incident on the hologram, H, at the second foci, f_2. The diffuser in the path of the object beam serves to uniformly illuminate the target. The reference wave, reflected from the beamsplitter, passes through a single, positive lens and a 25-μ pinhole, which

48

constitutes a spatial filter. This was necessary because of the inhomogeneity of the intensity of the normal-mode pulse from the laser. It, of course, then provides a uniformly intense divergent beam that is made incident on the film plane at H by the mirror M_2.

All parameters necessary for the description of the configuration are also labeled on this diagram. Using Figure 19 and Table 2 of system parameters, the various systems investigated will now be identified. System means the particular configuration including the wheel radius. A total of six systems are given in Table 2. The definition of systems 1 through 6 (Table 2) will be used throughout this discussion. Figure 20 is a photograph of one of the configurations used in which the location of the wheel is clearly visible.

Figure 21, a photograph of the ruby laser, shows the oscillator, amplifier cavity, and the limiting aperture between them, which, when properly aligned, serves two purposes. It produces a marked increase in the coherence length of the radiation, at the expense of intensity, and provides a more uniformly intense source. However, the homogeneity of the intensity is still unacceptable without the use of the spatial filter described earlier. Two pulses of different pulse lengths were obtained from this source, using the two available mode selections: normal and Q spoiled. Both of these pulses were detected and measured at the output of the spatial filter. Photographs and schematics of each are shown in Figures 22 and 23. The pulse length of the normal mode pulse was 2.5×10^{-4} s while that of the Q-spoiled pulse was four orders of magnitude shorter, 25×10^{-9} s. These values were monitored and stayed essentially constant for each shot. (This constancy was assured by the control of the water-coolant temperature and the period of flash-tube firing.)

A photograph of the two different radii wheels used as the target for systems 1 through 6 is shown in Figure 24. On the surface of the large wheel, r = 20.32 cm, it will be observed that a cross-hatched tape covers its entire periphery. This provided two purposes: (1) a definite markings whose detail could hopefully be resolved after motion, and (2) a dielectric-type surface as a reflector or scatterer instead of a metallic surface. A similar coating is found on the small wheel, r = 10.16 cm, except that here the white surface is a flat, diffuse white paint with vertical lines hand-painted on it. This serves the same two purposes described above; the reason for the painted surface will be explained later.

Figure 24 shows that the tape on the periphery of the large wheel appears to have a slight curvature along its height. This curvature is because the height of this taped surface is greater than the thickness of the wheel;

TABLE 2. PARAMETERS OF SYSTEMS INVESTIGATED

System	r^a (cm)	θ^b (deg)	$\delta_o{}^c$ (deg)	a^d (cm)	b^e (cm)	d^f (cm)	$\Delta \times \lambda/8^g$ (μ)	$\Delta \times \lambda/2^h$ (μ)
1	20.32	≈36	≈54	25.4	20.5	15	128	257
2	20.32	≈70	≈20	53.3	18.5	50	438	875
3	20.32	≈36	≈54	50.81	41	30	182	364
4	20.32	≈70	≈20	50.79	17.9	47.5	415	830
5	10.16	≈36	≈54	50.81	41	30	182	364
6	10.16	≈36	≈54	50.81	41	30	182	364

a. Radius of wheel used as object

b. Angle between b and a

c. Angle between a and perpendicular line to y axis
   (i. e., ellipse at point Q)

d. Semimajor axis of ellipse

e. Semiminor axis of ellipse

f. Separation distance from origin to either foci

g. $\lambda/8$ path length change of front illumination arm from
   laser to hologram

h. $\lambda/2$ path length change of front illumination arm from
   laser to hologram

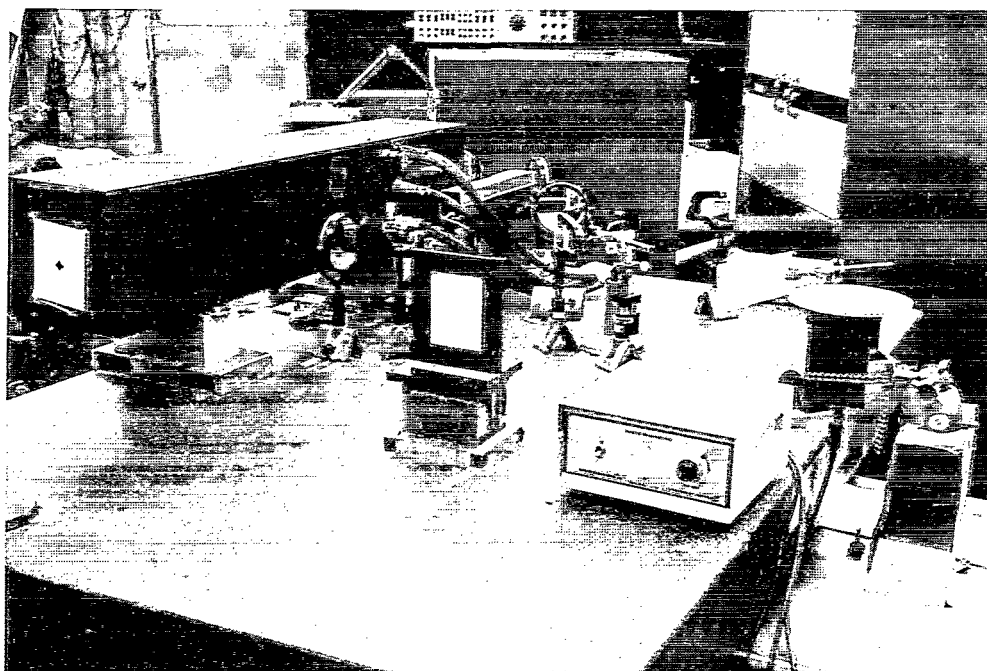Note: Systems 5 and 6 identical except for periphery of
      wheel.

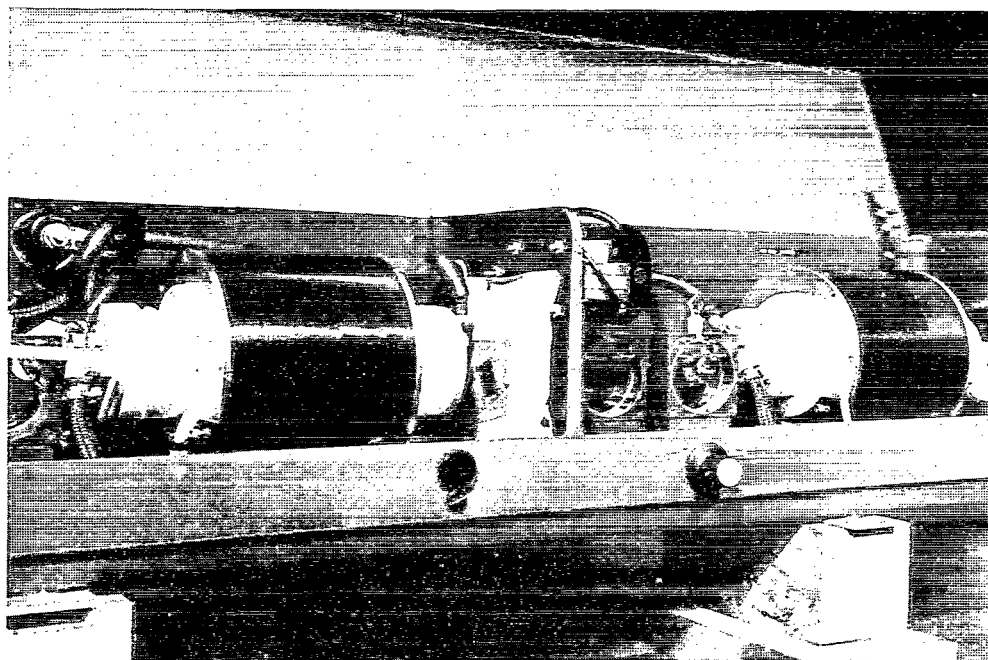Figure 20. Photograph of system showing wheel position

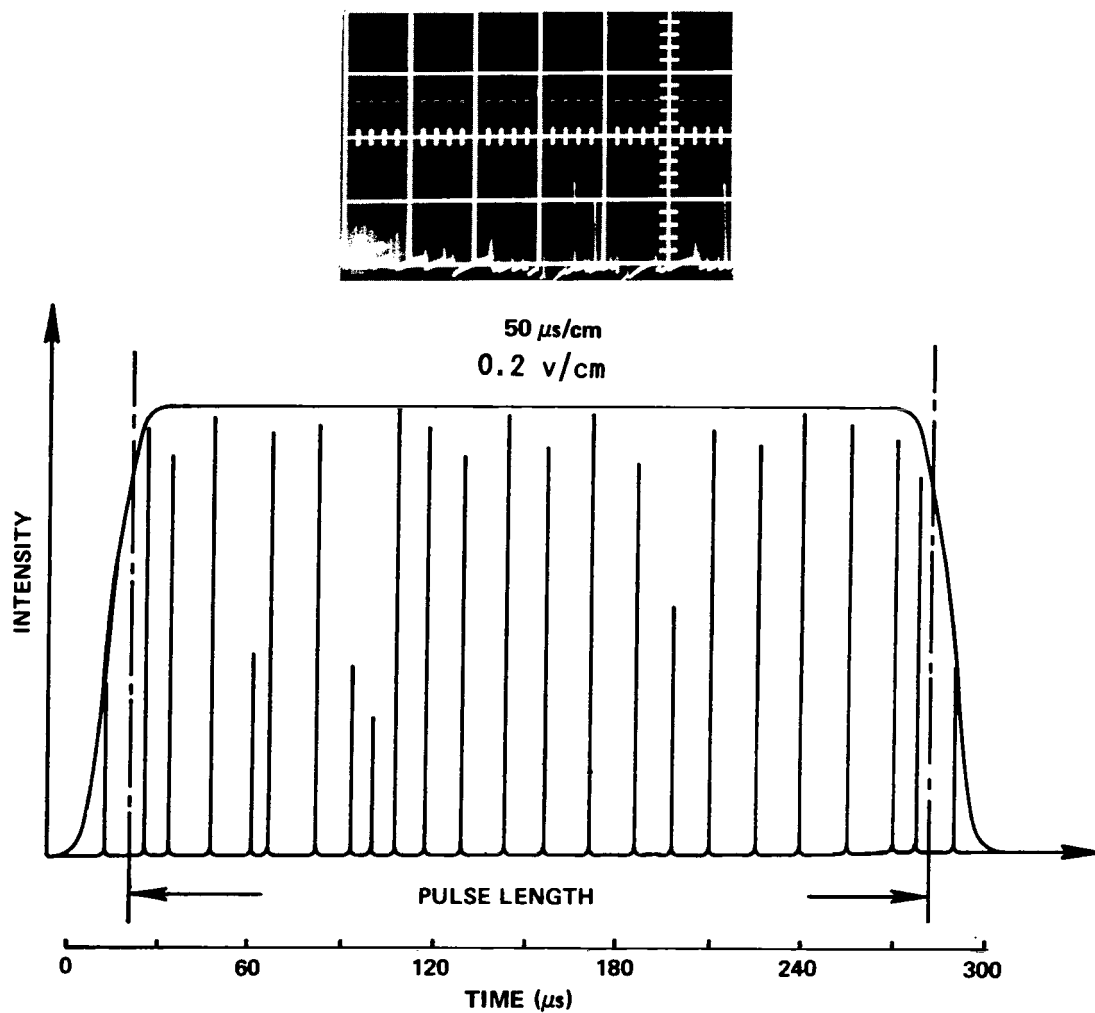Figure 21. Photograph of the ruby laser system

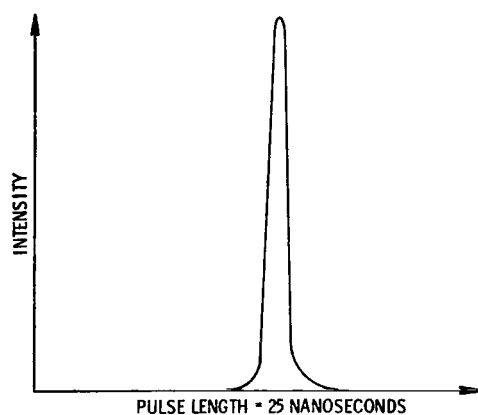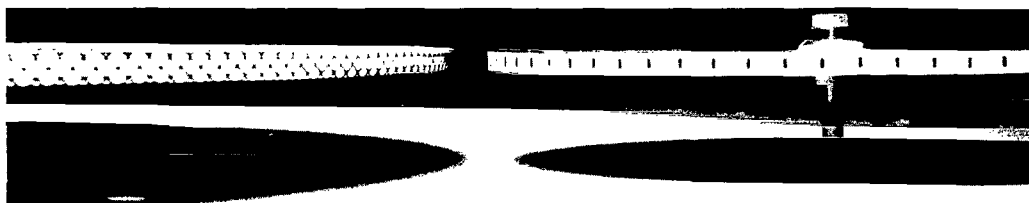Figure 22. Graphical description and photograph of normal mode pulse

Figure 23. Graphical description of Q-spoil pulse

Close-Up View of Wheels' Edges
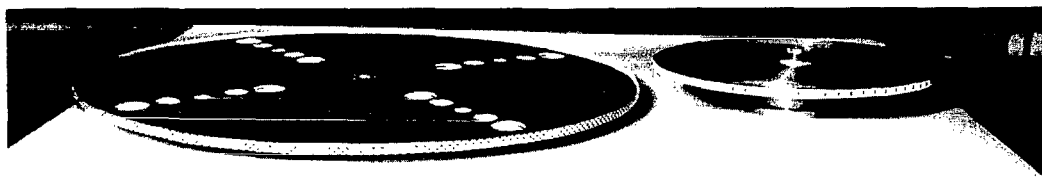
Figure 24. Photographs of two different radii target wheels

consequently, the tape on either side of the disc tends to bend toward the center of the disc. For the painted surface of the small wheel, this curvature does not exist. To ascertain the influence of this surface curvature of the tape, refer to Figure 25. The angle, β, is the total angle into which both wheels scatter the radiation originally incident at some point, Q. (Actually, this will be a solid angle, not a plane, β, but the hologram was 10.16 by 12.70 cm and it suffices to speak of an angle, β, in the x-y plane for this argument.) Now, the hologram in both cases intercepts an angle, $\epsilon < \beta$; i. e., the radiation is scattered over an angle, β, greater than the angle, ϵ, so the curvature of the surface is immaterial from this point of view. Of course, the magnitude of the angle, ϵ, will vary, depending on the magnitude of d or a, but ϵ is always less than β. The energy density at point P caused by radiation from Q is probably less for the curved surface disc since β for this disc was slightly greater than β for the flat wheel. However, this had little or no effect since the ratio of the beams at point P was controlled through the use of neutral-density filters. More will be said about the angle, ϵ, from a different point of view later.

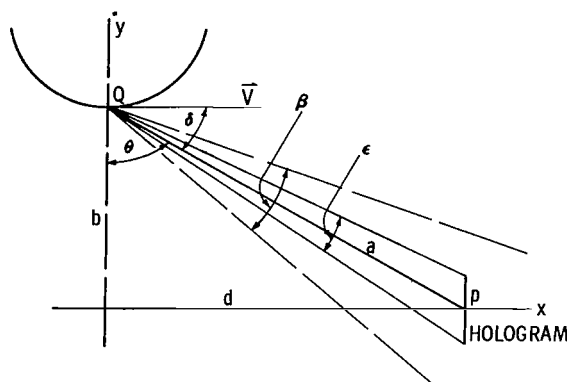Figure 25. Schematic of scattered
radiation.

The original plan for this investigation was to use the hybrid system described in Figure 13 with the back diffuser arm (see Subparagraph 1 of this section) and to record one hologram of a single projectile showing the resolution of front-surface detail. This approach was not pursued for the following reasons:

1. This approach would involve the engineering problem of designing a fairly complicated synchronization circuit to synchronize a nanosecond-type pulse with a high-speed event; namely, a projectile with v = 40 000 cm/s.

2. It was felt that the accomplishment of the above single shot provided very little insofar as the physics of the elliptical technique were concerned.

Therefore, in lieu of the above approach, a continuous-type target was chosen to obviate the need for a synchronization circuit and use a variety of slower velocities to better investigate the physics of the elliptical configuration; i. e., the influence of such parameters as d, a, θ, and δ (Table 2). To achieve high velocities as well as a continuous target, the decision was made to use a rotating disc, a gyroscope-type target. For the slower velocities, a dc continuously variable-speed motor was used to rotate the target disc. For the highest velocity, an ac motor taken from a Router tool was used. The upper limit on the angular speed of this motor was $\approx$417 rev/s. The angular speed of the disc attached to this motor was, of course, less than this because of air resistance.

The decision to use a rotating disc was further strengthened by the theory which shows (as well as experimental evidence, per Section IV.D.1) that the important parameter for motion holography is the total apparent distance, Δx, moved by the target during the exposure time; i. e., $\Delta x = v\tau$. Then the velocity per se is unimportant; its product with exposure time is the important parameter (other things being constant).

2. Comparison of the Experimental Results of the Systems Identified Above. Edge washout on both extreme edges of the target scene was noted to occur, primarily because all of the illuminated target does not lie along the line parallel and tangent to the chosen ellipse. For this particular problem, then, those points of the target are interesting which do not satisfy the chosen ellipse by virtue of their geometrical displacement from a line PP' tangent to the chosen ellipse. For simplicity, the disc is represented by a stack of two parallel plates, having a linear velocity, $\vec{V}$, directed parallel to PP' as the target

(Fig. 26). The points considered are S_1, S_0, and S_2. The angles δ_i and γ_i are the same as defined in Section III.C.1 (Fig. 8). From equation (37), one may write the exposure at point P as:

$$\mathscr{E}(P) = m\tau \left\{ K_c + E_r E_s \text{ sinc} \left[\frac{k\tau}{2} \vec{V} \cdot (\hat{a}_k - \hat{a}_p) \right] \cos \Phi \right\} . \qquad (110)$$
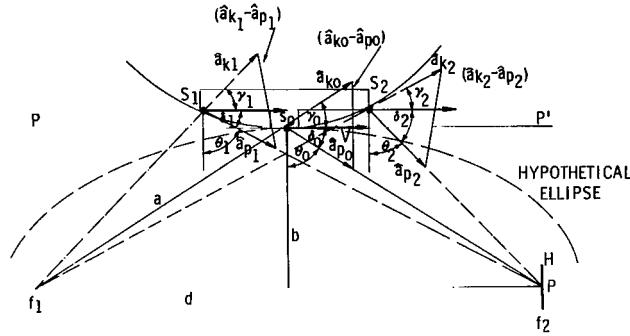
Figure 26. Variation of the sinc function caused by target geometry

The sinc function, which was thoroughly discussed in Section III, is that function caused by the motion which modifies the cosine fringes. Recall that if the argument of this function is zero, one has

$$\text{sinc } [0] \equiv 1, \qquad (111)$$

and obtains the brightest hologram. Any other value of the argument presents a degradation of the cosine fringes (Fig. 10).

One may write

$$\text{sinc } \left[\frac{k\tau}{2} \vec{V} \cdot (a_k - a_p) \right] = \text{sinc} \left[\frac{k\tau v}{2} (\cos \gamma - \cos \delta) \right] . \qquad (112)$$

Similarly, the respective sinc functions can be shown in Figure 26: for S_1,

$$\text{sinc} \left[\frac{k\tau v}{2} (\cos \gamma_1 - \cos \delta_1) \right] , \qquad (113)$$

for S_0,

$$\text{sinc} \left[\frac{k\tau v}{2} (\cos \gamma_0 - \cos \delta) \right] , \qquad (114)$$

55

and for S_2

$$\text{sinc}\left[\frac{k\tau v}{2}(\cos\gamma_2 - \cos\delta_2)\right] \qquad . \qquad (115)$$

From the symmetry of S_0 (Fig. 26),

$$\gamma_0 = \delta_0 \qquad . \qquad (116)$$

Furthermore, the following relations are clear (Fig. 26):

$$
\left.
\begin{aligned}
\gamma_1 &> \gamma_0 > \gamma_2 \\
\delta_1 &< \delta_0 < \delta_2 \\
\delta_2 &> \gamma_0 \\
\delta_1 &< \gamma_0
\end{aligned}
\right\} \qquad . \qquad (117)
$$

Additionally, in all three cases the total angle between $\hat{a}_k$ S $\hat{a}_p = \gamma + \delta$.
Then, one may write,

$$\beta' = \gamma + \delta \qquad . \qquad (118)$$

Now, consider a hypothetical case to evaluate the sinc function for S_1, S_0, and S_2 of the target in Figure 26. As the chosen ellipse, the parameters are taken of system number 2 (Table 2) which demand that, at the point of symmetry (i. e., S_0 of the system),

$$\delta_0 = 20 \text{ deg} \qquad ,$$

$$\gamma_0 = 20 \text{ deg} \qquad , \qquad (119)$$

and

$$\theta_0 = 70 \text{ deg} \qquad .$$

Then, let

$$\beta' \equiv \delta_0 + \gamma_0 = 40 \text{ deg} \qquad . \qquad (120)$$

It is assumed that the target is sufficiently long and displaced from PP' at S_1 and S_2 such that, e. g.,

$$\delta_1 = 10 \text{ deg}$$

and

$$\delta_2 = 30 \text{ deg} \qquad . \tag{121}$$

Then, from equations (120) and (121),

$$\beta' = 40 \text{ deg} = \gamma_1 + \delta_1 \qquad , \tag{122}$$

$$\gamma_1 = 40 \text{ deg} - \delta_1 \qquad ,$$

or

$$\gamma_1 = 30 \text{ deg} \qquad . \tag{123}$$

Also, by the same reasoning,

$$\gamma_2 = 10 \text{ deg} \qquad ,$$

and, from equations (113), (114), and (115), the respective sinc functions become: for S_1,

$$\text{sinc} \left[\frac{k\tau v}{2} (\cos 30 \text{ deg} - \cos 10 \text{ deg}) \right] \qquad , \tag{124}$$

for S_0,

$$\text{sinc} \left[\frac{k\tau v}{2} (\cos 20 \text{ deg} - \cos 20 \text{ deg}) \right] , \tag{125}$$

and for S_2,

$$\text{sinc} \left[\frac{k\tau v}{2} (\cos 10 \text{ deg} - \cos 30 \text{ deg}) \right] \qquad . \tag{126}$$

Therefore, since $v\tau = \Delta x$ for S_1, one has

$$\text{sinc} \left[(-0.019) \frac{k\Delta x}{2} \right] \neq 1 \quad , \tag{127}$$

for S_0,

$$\text{sinc} \left[(0) \frac{k\Delta x}{2} \right] \equiv 1 \quad , \tag{128}$$

and for S_2,

$$\text{sinc}\left[(0.019)\,\frac{k\Delta x}{2}\right] \neq 1 \quad. \tag{129}$$

It is then seen that edge washout occurs because of this variation of the sinc function that modifies the cosine fringes. It is further observed that this degradation occurs in an equally displaced fashion about the symmetrical point of the chosen ellipse (i. e., the S_0 point). This same fact, of course, is implied in Figure 10, where the direction of illumination with respect to the velocity vector was varied and plotted the value of the argument of the sinc function. It is noted here, and will be shown later, that this is precisely what happens experimentally.

It is clearer from this discussion and Figure 26 that the same type of phenomena would occur even if the target were not displaced; i. e., if it were parallel and coincident with the line, PP', that is tangent to the chosen ellipse, provided the targets were long enough. But, in terms of the elliptical description, one would simply say that the long target does not sufficiently approximate the chosen elliptical surface. Then, again, agreement exists between the vectoral description and the elliptical description. However, this phenomenon of edge washout is not so startling since the allowed size of the target is certainly determined by the choice of the parameters or size of the chosen ellipse.

The systems (numbers 1 through 6) identified in Section IV.D.1 will be compared. Each system has the geometrical parameters displayed in Table 2 and was tested in the following fashion.

To establish a reference between the condition of a stationary target and that of a moving target, the first hologram taken for each system was that of its respective stationary target. Ultimately the measured value, $\overline{S}_i$, of each hologram was divided by the respective value of $\overline{S}_i$ for its stationary target.

Equation (86) was used to calculate the value of $\Delta x_{\lambda/8}$ for each system sufficiently to cause a path-length shift of $\lambda/8$ in the front-surface illumination arm (Table 2). From equation (87), since

$$v = \frac{\Delta x}{\tau} \quad, \tag{130}$$

it was ascertained that the velocity, $v_{\lambda/8}$, was necessary to cause a $\lambda/8$ shift in this path length of each system. Then, using

$$\frac{v}{r} = \omega \quad , \tag{131}$$

the rotational speed was determined sufficiently as to allow the desired tangential velocity employed to approximate a linear velocity. Of course, the same procedure allows determination of the proper rotational speed sufficient to cause a $\lambda/2$ shift in the front-surface illumination arm.

Two more holograms then were acquired in which the target moved the distance $\Delta x_{\lambda/8}$ and $\Delta x_{\lambda/2}$, respectively, during the exposure time of 2.5×10^{-4} s, which was constant for all shots of all systems tested. Two exceptions to this exposure time occurred in system numbers 2 and 5, which will be explained later. From the value of ω determined above, the frequency of the rotating wheel was accurately set through the use of a strobetachometer, calibrated to within 1 percent of the value being measured. This approach was followed systematically for all systems tested.

Therefore, using a pulse length or exposure time which was constant for all systems, the following holograms of the target wheel for each system were obtained:

1. The stationary target wheel.

2. The target wheel as it moved a distance, $\Delta x_{\lambda/8}$, sufficient to shift the path length of $\lambda/8$ for that system.

3. The target wheel as it moved a total distance, $\Delta x_{\lambda/2}$, for that system.

Actually, holograms were taken with a $\Delta x > \Delta x_{\lambda/2}$ for each system, but only the holograms mentioned above for system numbers 1, 3, and 4 will be compared, since these particular holograms have values of path-length shift that are common to all of them. However, in an effort to demonstrate the effect of edge washout discussed earlier, a total of eight holograms for system number 2 will be discussed. Two holograms each of system numbers 5 and 6 will be discussed separately.

After developing all of the holograms in the manner discussed in the Appendix, photographs were taken of the image produced by each hologram

during reconstruction. All images were placed in a one-to-one correspondence with their original target, the target being the same for all systems. The resultant negatives, whose development was carefully controlled, were then used to measure the amount of front-surface detail resolved in each case. These measurements were made in the following way.

Since each target wheel had a pattern on its periphery, the resultant negative of the image of this pattern was viewed to determine a position that would be used as the limit of resolved detail for each image on the negatives. A densitometer was then used to determine the density of this point and to locate the position of corresponding density on the opposite side of the image. At these precise positions on the negative, a hair-thin line was drawn with a knife edge. This particular value of the density was found for all the other negatives and, again, a fine line was drawn. It should be pointed out that the density of all holograms and photographs was held constant so that the only influence on the density of each was determined by the reduction in brightness of the image caused solely by the motion of the target itself during the exposure time.

Each negative was then aligned on the stage of a spectrum-line comparator, where a visual display of the resolved pattern, magnified up to 10 times, was presented on a screen. The position of the fine line, drawn on the negative, was electronically determined by a trace on the cathode-ray tube of the spectrum-line comparator (Fig. 27). Using this instrument, the length of the image lying between the fine lines was measured several times and an average value taken, thereby obtaining an average quantity, $\overline{S}_i$, for each negative

corresponding to each hologram of the specific system tested. The values of $\overline{S}_i$ for each hologram of all six systems tested are listed in Table 3 and represent the average of the length of the resolved detail of each image.

Since the stationary target of each system is the reference between the condition of motion versus no motion of the target for that system, another quantity, $\overline{S}_{0_i}$, is defined for each system:

$$\overline{S}_{0_i} \equiv \frac{\overline{S}_i \text{ (for motion case)}}{\overline{S}_i \text{ (for stationary case)}} \quad ; \qquad (132)$$

i. e., $\overline{S}_{0_i}$ is just the average length of each resolved image, relative to the
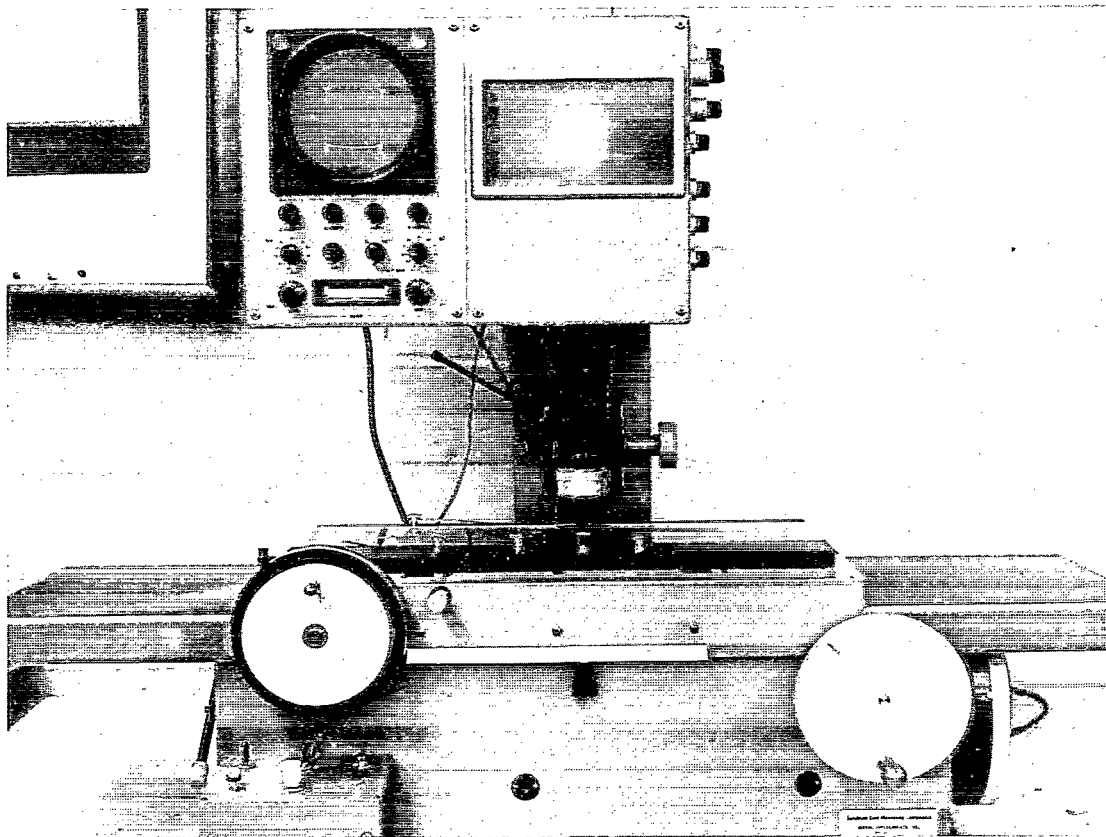
Figure 27. Photograph of spectrum line comparator

average length of the stationary image, for each respective system. This is necessary since the length of the image resolved is certainly dependent upon the length of the image illuminated; this illuminated length was unavoidably different for each system tested. Then, $\overline{S}_{0_i}$ denotes the amount of the original stationary object resolved by each successive hologram of a given system. All of the values of $\overline{S}_{0_i}$ are listed in Table 3 for each respective system.

From the theory of the elliptical holographic system it can be seen that the total allowed travel, Δx, is definitely a function of the system parameters, a, b, and d; i. e., for a given specific value of travel Δx, the effect of this motion in terms of the degradation of image quality will be less for a làrge ellipse than for a small ellipse, other things being constant. Shortly, experimental evidence to support this theoretical contention will be presented.

TABLE 3. SUMMARY OF EXPERIMENTAL RESULTS AND PARAMETERS

System	$\bar{S}_i$ (cm)	$\bar{S}_{0i}$ (cm)	Δx_i (μ)	V_i (cm/sec)	θ (deg)	δ_0 (deg)	d (cm)	a (cm)	$\dfrac{a\,1/2}{\cos\theta}$ (cm)^2
H-1	8.955	1							
H-2	5.895	0.658	128	52	36	54	15	25.4	6.22
H-3	5.330	0.595	257	102					
H-4	4.625	0.516	715	286					
H-5	6.380	1							
H-6	5.530	0.867	255	102					
H-7	4.950	0.776	438	175					
H-8	3.885	0.609	875	350	70	20	50	53.3	21.35
H-9	4.160	0.652	715	286					
H-10	2.120	0.332	2250	900					
H-11	1.070	0.168	4240	1696					
H-12	6.320	0.991	0.424	1696					
H-13	11.235	1							
H-14	8.455	0.752	182	73	36	54	30	50.81	8.81
H-15	6.030	0.537	364	146					
H-16	6.350	1							
H-17	4.930	0.776	438	174	70	70	47.5	50.79	20.89
H-18	3.873	0.609	875	348					
H-19	4.503	1							
H-20	3.003	0.667	4.4	17 546	36	54	30	50.81	8.81
H-21	5.230	1							
H-22	3.402	0.651	4.4	1.75	36	54	30	50.81	8.81

Figure 28 presents eight photographs showing the images resolved for eight successive holograms taken with system number 2. Each photograph represents successively larger motions; i. e., values of Δx. Photograph number H-5 is of the stationary target. Photographs H-6 through H-11 represent successively larger motions, all with the same constant exposure time of 2.5×10^{-4} s. These photographs vividly display the effect of edge washout discussed earlier. Photograph number H-12 is a Q-spoil exposure, $\tau = 25 \times 10^{-9}$ s, and is the result of the same motion as for photograph H-11. Because of the four orders-of-magnitude difference in the exposure time, the resolved detail is strikingly different. Therefore, it is obvious that the stop action is a function of exposure time; other things being constant. Consequently, in the following it will be recalled that the exposure time of 2.5×10^{-4} s was constant in all systems except for system number 5, which will be discussed separately. Additional information is included in the caption for each photograph of Figure 28.

H5   STATIONARY

H8. ΔX_i = 875μ
       V_i = 350 cm/s

H6 ΔX_i = 255μ
      V_i = 102 cm/s

HIO: ΔX_i = 2,250μ
       V_i = 900 cm/s

H7 ΔX_i = 438μ
      V_i = 175 cm/s

HII ΔX_i = 4,240μ
       V_i = 1696 cm/s
       T = 2.5 x 10^{-4} s

H9 ΔX_i = 715μ
      V_i = 286 cm/s

HI2. ΔX_i = 0.424μ
       V_i = 1696 cm/s
       T = 25 x 10^{-9} s
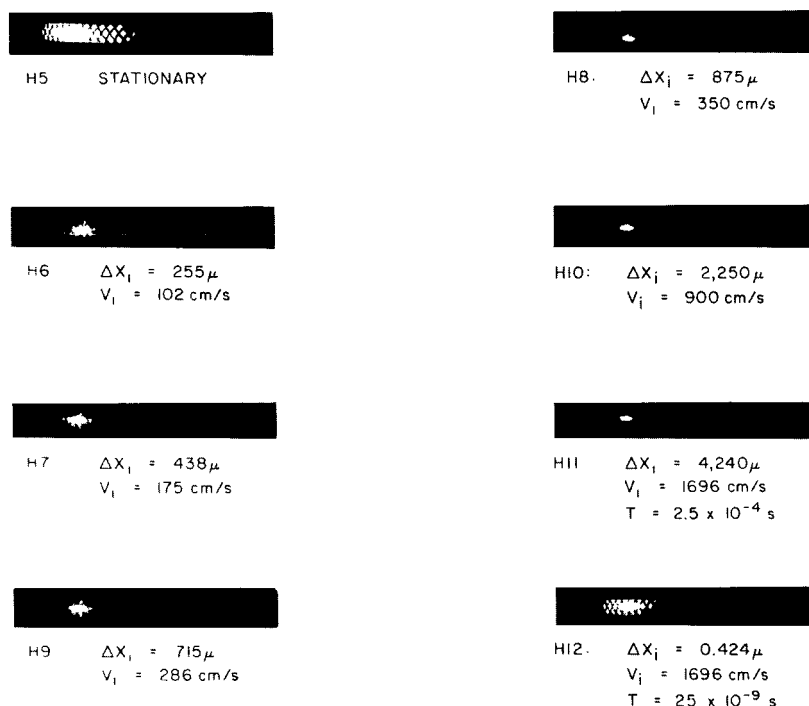
Note: For H-5 through H-11, $\tau = 2.5 \times 10^{-4}$ s

Figure 28. Photographs for largest "d" system
number 2, H-5 through H-12

Experimental verification that the stop action is indeed a function of the elliptical system configuration will now be presented.   Consider the following data from Table 3:   For H-3, with parameters

$$d = 15 \text{ cm}$$

$$a = 25.4 \text{ cm}$$

$$\theta = 36 \text{ deg}$$

$$\Delta x = 257 \ \mu \qquad\qquad\qquad (133)$$

$$v = 102 \text{ cm/s}$$

$$\tau = 2.5 \times 10^{-4} \text{ s} \qquad ,$$

one has

$$\overline{S}_{0_3} = 0.595 \qquad .$$

For H-6, with parameters

$$d = 50 \text{ cm}$$

$$a = 53.3 \text{ cm}$$

$$\theta = 70 \text{ deg}$$

$$\Delta x = 257 \ \mu \qquad\qquad\qquad (134)$$

$$v = 102 \text{ cm/s}$$

$$\tau = 2.5 \times 10^{-4} \text{ s} \qquad ,$$

one has

$$\overline{S}_{0_6} = 0.867 \qquad . \qquad\qquad\qquad (135)$$

64

Then, since

$$\bar{S}_{0_6} = 1.48\,\bar{S}_{0_3} \qquad , \tag{136}$$

and since the only parameters that differ for these two cases are those defining the different systems, one must conclude that the differences observed in the magnitude of the relative average value of the resolved image must be because of some function of the elliptical system itself; i. e., in the orientation of the holographic system used. A second such comparison may be made using H-4 and H-9, whose parameters and data are found in Table 3. Observe that the magnitude of the relative average value for H-4 is

$$\bar{S}_{0_4} = 0.516 \qquad , \tag{137}$$

while that for H-9 is

$$\bar{S}_{0_9} = 0.652 \qquad ; \tag{138}$$

then, in this case,

$$\bar{S}_{0_9} = 1.26\,\bar{S}_{0_4} \qquad . \tag{139}$$

From a comparison of parameters of the systems found in Table 3, the total travel, $\Delta x = v\tau$, is the same for both systems, in spite of the difference in magnitude of the relative average value for each. It must again be concluded that this oberserved difference is caused solely by system dependence. Furthermore, it is observed that the larger the system is (i. e., the larger the value of d), it always allows the larger relative length, $\bar{S}_{0_i}$.

As further evidence of this last statement, consider the results for a path-length shift for three successively larger ellipses. For H-2, with d = 15 cm and other parameters given in Table 3, the magnitude of the relative average value of the resolved image is:

$$\bar{S}_{0_2} = 0.638 \qquad ; \tag{140}$$

for H-14, with d = 30 cm,

$$\overline{S}_{0_{14}} = 0.752 \quad ; \quad$$ (141)

and, finally, for H-7, with d = 50 cm,

$$\overline{S}_{0_7} = 0.776 \quad . \quad$$ (142)

Yet one notes from an inspection of parameters that the range of the value of d (cm) for these three systems is:

$$15 \leq d \leq 50$$ (143)

and the allowed range of total travel, $\Delta x_{\lambda/8}$, sufficient to shift the optical path length in each system by a constant amount, $\lambda/8$, is:

$$128 \, \mu < \Delta x_{\lambda/8} < 438 \, \mu \quad , \quad$$ (144)

respectively, as indicated by equation (86); i. e., the larger ellipse allows the scene to travel farther during the exposure time before the total phase shift of the optical path-length changes by $\lambda/8$. Yet, in spite of this increase in the total allowed travel, $\Delta x_{\lambda/8}$, the ability of the larger system to resolve detail from the target, as indicated by the $\overline{S}_{0_i}$ value, increases or at least stays approximately constant for the succesively larger ellipses.

If the results of a $\lambda/2$ path-length change for these same systems is considered, one sees essentially the same result as noted above — the ability of the larger system to resolve detail from the moving scene, as indicated by the quantity $\overline{S}_{0_i}$ of Table 3, increases or at least stays approximately constant for the successively larger ellipses. This occurs in spite of the fact that the total travel, $\Delta x_{\lambda/2}$, necessary to cause a $\lambda/2$ path-length change is necessarily larger for the larger ellipses.

Having established that the stop action is indeed a function of the system, one may ask the question: What is the form of this function? To answer this, one must compare two systems having identical values of the angle, θ, but different values of the length, a; also, compare two systems having approximately equal values of the length, a, but different values of the angle, θ.

For the case of two different systems having the same value of the angle, θ, but different values of semimajor axis, a, we point out systems 1 and 3 with $\theta = 36$ deg and other parameters as given by Table 3. Then, on comparing the results for Δx_i and $\overline{S}_{0_i}$ of H-1, H-2, and H-3 of system 1 with those for H-13, H-14, and H-15 of system 3, it may be seen that the allowed increase in total travel, Δx, for a constant value of path-length change is caused primarily by the difference in the values of parameters d and a for the two systems.

Likewise, for two systems with a semimajor axis of a ≈ 50.81 cm but different values of the angle, θ, the results for Δx_i and $\overline{S}_{0_i}$ of H-13, H-14, and H-15 of system 3 are compared with the results of H-16, H-17, and H-18 of system 4. Now, it can be seen the allowed increase in Δx is caused primarily by the difference in the value of parameters d and θ for these systems. Therefore, the desired functional dependence must be of the form f(d, a, θ).

Recalling equation (86) for Δx,

$$\Delta x = \left(\frac{\Delta L}{2}\right)^{\frac{1}{2}} \frac{a^{\frac{3}{2}}}{b} \quad , \tag{145}$$

and, from Section IV.A., it is clear that

$$\Delta L = 2 \Delta a \tag{146}$$

and

$$\frac{a}{b} = \sec \theta = \frac{1}{\cos \theta} \quad . \tag{147}$$

Then, equation (145) may be written as:

$$\Delta x = (\Delta a)^{\frac{1}{2}} \frac{a^{\frac{1}{2}}}{\cos \theta} \tag{148}$$

or

$$\Delta x \; \alpha \; \frac{a^{\frac{1}{2}}}{\cos \theta} \quad , \tag{149}$$

67

where θ is the angle between b and a of the ellipse. Then, it can be seen that the analytical equation (86) derived for our hypothetical ellipse has the desired functional form that satisfies the results observed experimentally. The value of this function, given in equation (149), for all systems tested is given in Table 3 and is seen to increase for each system having a larger value of the parameter d. Figure 29 presents photographs showing the results of system number 1, the smallest system tested. (Figure 28 has already shown the largest system tested — system number 2.)
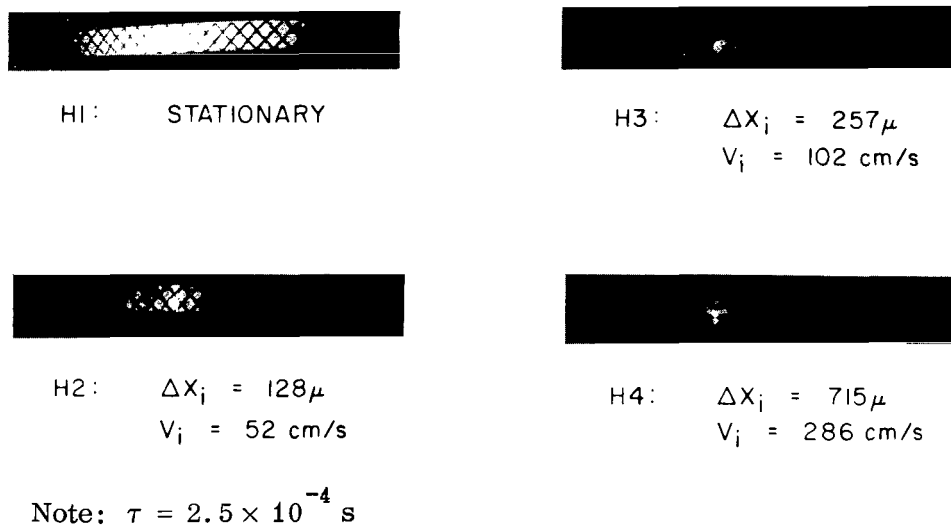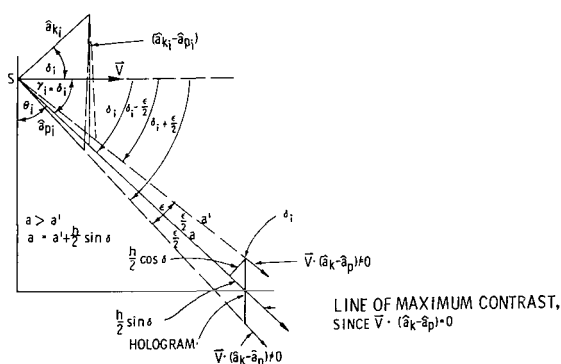
HI: STATIONARY

H3: ΔX_i = 257μ

          V_i = 102 cm/s

H2: ΔX_i = 128μ

         V_i = 52 cm/s

H4: ΔX_i = 715μ

         V_i = 286 cm/s

Note: $\tau = 2.5 \times 10^{-4}$ s

Figure 29. Photographs for smallest d system number 1, H-1 through H-4

Attention is now directed back to the discussion of Section IV. D. 1. , where mention was made of an angle, ϵ, and Figure 25 where the effect of the variation of the sinc function was discussed. It is intended at this point to demonstrate a connection between the parameters a and θ with the angle, ϵ, and another effect of the variation of the function (Fig. 30).

Figure 30. Relation between parameters a and ϵ and variation of sinc function

68

From this figure, one can write

$$\frac{\epsilon}{2} = \tan^{-1}\left(\frac{\frac{h}{2}\cos\delta}{a - \frac{h}{2}\sin\delta}\right) \quad , \tag{150}$$

where h is the dimension of the hologram plate. From this relation, it is readily seen that as a increases, the value of $\epsilon/2$ decreases, and the effect caused by the variation of the sinc function is reduced from some maximum — additional evidence that the larger system tolerates higher motion.

Experimental verification of the theoretical conclusion that the total allowed motion, $\Delta x = v\tau$, is the primary parameter affecting image degradation caused by scene motion is now presented. Consider system numbers 5 and 6 whose system parameters are identical. The sole difference is in the type of surface found on the periphery of the target wheel in each case. The periphery of the wheel of system number 5 is composed of a flat, diffuse, painted background on which vertical bars have been painted, It was necessary to use a painted surface since the tangential velocity of this wheel was so high that the tape attached to it exploded after a certain velocity was reached. The periphery of the target wheel in system number 6 was composed of white tape with inked vertical bars; the vertical bars on this surface are slightly narrower than the painted ones of system number 5. Furthermore, the surface of system number 5 is more diffuse than that of system number 6.

With this sole exception in mind, the otherwise identical parameters of system numbers 5 and 6 are presented in Table 2 and 3. System numbers 5 and 6 have the following parameters:

$r = 10.16$ cm

$\theta = 36$ deg

$\delta = 54$ deg

$a = 50.81$ cm

$b = 41$ cm

$d = 30$ cm

$\Delta x = 4.4 \mu = v_5\tau_5 = v_6\tau_6$

$$\frac{a^{\frac{1}{2}}}{\cos\theta} = 8.81$$

$$\overline{S_0}_{20} = 0.667; \quad S_0{}_{22} = 0.651$$

Other than the periphery surface, the sole difference between the two systems is found in the individual values of velocity and exposure time or pulse length; i. e.,

<table>
<tr><td>System Number 5</td><td>System Number 6</td></tr>
<tr><td>$v_5 = 1.7546 \times 10^4$ cm/s</td><td>$v_6 = 1.76$ cm/s</td></tr>
<tr><td>$\tau = 25 \times 10^{-9}$ s</td><td>$\tau = 2.5 \times 10^{-4}$ s $= \tau_5 \times 10^{-4}$</td></tr>
</table>

The value of Δx is identical for both, while the velocity and exposure time of each differ by four orders of magnitude. It is further noted that the respective values of the relative average length parameter, $\overline{S_0}_i$, is approximately

equal. Photographic evidence of this is shown in Figure 31, where the results of the systems 5 and 6 are presented. Notice that for the highest velocity of 1.75×10^4 cm/s, the second smallest system tested and therefore one of the worst systems available to us was used.

Figure 31. Photographs for system numbers 5 and 6

Since it has been verified that the value of Δx is the important parameter in this study of motion holography, one now finds the second highest value of Δx obtained in this study. Of course, H-10 of system 2 is selected since here the limit is certainly being approached, as evidenced by the blur of the pattern resolved (Fig. 28). For H-10,

$$\Delta x = 2250\,\mu = v\tau \qquad .$$

Now, recall that this value was the result of a velocity equal to 900 cm/s and an exposure time of 2.5×10^{-4} s. Suppose one attempts the same shot with an exposure time four orders of magnitude shorter; i. e., 25×10^{-9} s (Q-spoil pulse) and retains all parameters identical to those for H-10. In view of the last results, what limiting upper velocity could the system allow such that we would obtain at least the same resolution offered by H-10? From Table 3, for H-10,

$$\Delta x = 2250\,\mu = v\tau \ , \tag{151}$$

using the Q-spoil pulse length,

$$v = \frac{2250 \times 10^{-4}\ \mathrm{cm}}{25 \times 10^{-9}\ \mathrm{s}} \ , \tag{152}$$

and

$$v = 90 \times 10^{5}\ \mathrm{cm/s} \qquad . \tag{153}$$

Then, even using a safety factor of one order of magnitude, the limiting upper velocity would be,

$$v = 9 \times 10^{5}\ \mathrm{cm/s} \quad . \tag{154}$$

Therefore, for a system having parameters identical to those of system number 2, this velocity represents the upper limit of velocity using a Q-spoil pulse of 25×10^{-9} s. The predicted results of such a velocity will be at least as good as the results shown by H-10 of Figure 28 and Table 3, and probably as good as H-8, in view of the above order-of-magnitude change.

V. SUMMARY AND CONCLUSIONS

Various types of holography have been presented and discussed, theoretically and experimentally, including the time-variant effects caused by motion. A holographic system, unique in its configuration, has been discussed that allows the resolution of front-surface detail from scenes moving at high velocity. The highest velocity for which front-surface detail was experimentally resolved was 1.75×10^4 cm/s; however, it has been inferred from the comparison of system numbers 5 and 6 that front-surface detail could be resolved even for scenes with very high velocities. These very high velocity cases have yet to be accomplished experimentally. However, before this work, the highest-scene velocity from which front-surface detail was obtained has been a few centimeters per second. For this experiment, the scene velocity was the tangential velocity of the rim of a rotating wheel. The degree to which this approximates linear velocity is denoted by the fact that for the largest total displacement, Δx, of the scene, $\Delta x = 4240\ \mu$, (the angle of wheel rotation) was only 1.2 degrees.

From the experimental results of this investigation, it may be concluded that:

1. The total scene motion during exposure, $\Delta x = v\tau$, is the parameter of importance for motion holography; i. e., the product of velocity and time.

2. The degradation of the cosine fringes caused by the scene motion during exposure causes the scene detail to blur out. Furthermore, this blurring or edge washout occurs symmetrically about the point of the target that is tangential to the surface of the hypothetical ellipse. (This was also shown theoretically in terms of the sinc function.)

3. The allowed motion or stop action of the moving scene is definitely a function of the elliptical arrangement used that defines the holographic system. The functional form of this system dependence for travel in the $\vec{x}$-direction has been shown to be proportional to $a^{1/2}/\cos\theta$; the value of this function for all systems tested has been tabulated.

4. The ability to allow larger total motion, Δx, for a given optical path-length shift, during a constant exposure time is found to increase with the size of the holographic system being used.

Although it was not experimentally concluded, it is believed that one may reasonably infer from comparison of the data of this investigation that good front-surface detail can be resolved from a scene traveling at velocities,

$$v = 9 \times 10^5 \text{ cm/s} \qquad ,$$

if one uses the system configuration similar to that discussed in Section IV. It is also believed that the detail obtained from a target having this velocity would probably be as good as that shown by photograph H-8 of Figure 31.

George C. Marshall Space Flight Center
National Aeronautics and Space Administration
Marshall Space Flight Center, Alabama   June 30, 1971
905-35-13-0000

APPENDIX. THE ROLE OF PHOTOGRAPHY
IN THE HOLOGRAPHIC PROCESS

One of the most important elements in the holographic process is the photographic emulsion; i. e., the various recording media in which the interference pattern is stored. A replica of this interference pattern produced by the scattered wave from the object and the coherent reference wave must exist as detectable changes in some physical medium to constitute a hologram. In most cases, the interference pattern is recorded in the medium in one of two forms: (1) an optical density pattern in which the material is absorptive and the hologram recorded is a density grating that diffracts light by modulating the intensity of the reconstruction beam (this is the most commonly used in Fresnel or Fraunhofer types of holography, although its diffraction efficiency is ≤ 4 percent), or (2) as a phase-shift pattern, in which the material is nonabsorptive or phase only, and the hologram has a uniform optical density. The phase variation of the recording media diffracts light in a similar manner to a phase grating. For phase-only materials, the required phase shift of the reconstruction wave is provided through the local variations in the thickness and/or the refractive index of the recording medium.

Among the various recording media used for the holographic recordings are [28, 29, 32]:

1. Photographic emulsions — These emulsions are basically absorptive media. However, they can be bleached with ammonia, after proper development, and the phase-only term will remain.

2. Photochromic materials — These materials have the economic advantage that they can be erased and used several times. The materials contain absorptive color centers and most of them are sensitive only in the shorter wavelength region of the visible spectrum and in the ultraviolet. They usually have high-resolution capabilities and low-scattering noise; yet, they have low sensitivity.

3. Photopolymer materials — Such materials include photosensitive resist and other organic materials that have the property of changing from monomer to polymer because of exposure to light. After exposure, the materials show either a differential index of refraction or a differential solubility to a solvent. Therefore, holograms recorded on these materials are phase-only holograms. With certain materials, holograms can be recorded without the need for chemical development and fixing; therefore, this process has the advantage of real-time holography.

74

4. Thermoplastic materials — These materials respond to an electro-static force and form a phase image from the charge-induced deformation. These are said to have high sensitivity and low-scattering noise.

5. Dichromate-sensitized gelatin — These materials are believed to be sensitized by a process of reducing the dichromate ion Cr^{+6} to Cr^{+3} by exposure to light to form a complex that hardens the gelatin. A phase image is formed by dissolving the unhardened gelatin.

6. Electro-optical crystals — Lithium niobate was the first crystal used for hologram storage. A suitable intense beam from an argon laser produces refractive index changes in the crystal. Erasure of the hologram is achieved by heating the crystal to 170°C after which the crystal can be reused.

Table A-1 summarizes the recording media used holography.

Since photographic emulsions are the most commonly used recording medium for holography, it is now appropriate to discuss this medium in some detail.

Probably, the two main properties that make photographic material suitable for holography are its color sensitivity and its resolving power. To record the laser radiation, the photographic emulsion must be sensitive to the laser's particular monochromatic radiation. The two most important laser lines are 6328Å (HeNe) and 6943Å (ruby); then, since most panchromatic materials have passed through their maximum sensitivity at these lines, special sensitizers must be used. Because of the mechanical rigidity requirements of holography, the base used is usually a glass plate. Two readily available sources for holography are: Kodak 649 F spectroscopic plates with a resolution >3000 lines/mm and the Agfa Gavaert which supplies a range of specially sensitized emulsions that allow exposures of a fraction of a second.
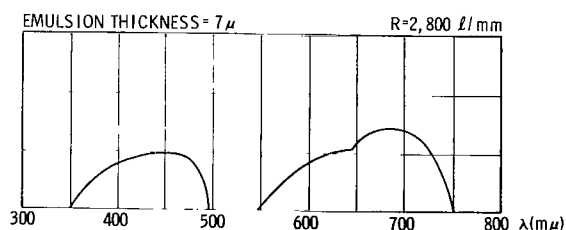
The medium used in the present experiment was the Agfa Gavaert plate 10-E-75 that is sensitized especially for the ruby line, 0.6943 μm. A plot of its sensitivity is shown in Figure A-1.

Figure A-1. Spectrogram for artificial light (3200° K), Scientia 10-E-75

TABLE A-1. PROPERTIES OF RECORDING MEDIA

Recording Medium	Typical Resolution (lines/mm)	Typical Exposure Required (ergs/cm²)	Absorptive (A) or Phase Only (P)
Photographic Emulsions	>2000	$20 - 10^3$	A and P
Photochromic Materials	>2000	$10^5 - 10^7$	A
Photopolymer Materials	>1000	$10^4 - 10^6$	P
Thermoplastic Materials	>1000	$10 - 100$	P
Dichromate-Sensitized Gelatin	>2000	10^5	P
Electro-optical Crystals	>4000	10^9	P

The resolving power of emulsions can be explained in the following way. The distance on the hologram between a line of high density and one of low density corresponds to the difference in path length between the reference beam and the object beam of $\lambda/2$.

If Φ is the angle between the reference beam and object beam when they are incident on the photographic plate, the distance between two dark lines is given by

$$d = \frac{\lambda}{2 \sin \Phi/2} \quad ,$$

where λ is the wavelength of the incident radiation. The results of this in terms of $1/d$ (i. e., in lines per millimeter) are given in Table A-2 for 3 deg $\leq \Phi/2 \leq 50$ deg.

TABLE A-2. MINIMUM FILM RESOLUTION (LINES/mm)

Angle (deg)	Laser-Emission Wavelength				
	3473 Å	4880 Å	5145 Å	6328 Å	6943 Å
2	100	72	68	60	50
4	201	143	136	120	101
6	302	215	204	170	151
8	400	285	270	220	200
10	501	357	338	290	251
15	746	531	503	409	373
20	987	702	667	580	493
25	1217	866	822	668	609
30	1439	1024	972	790	720
40	1851	1317	1250	1016	926
50	2206	1570	1489	1210	1103

As stated before, the photographic emulsion is an absorptive medium. When the material is exposed to light, developable centers are formed on the silver halide grains inside the gelatin emulsion. In the development process, silver grains are formed from these centers. The portion of the emulsion that receives more exposure will have more silver grains developed. After completion of the fixing process, which removes the unexposed sensitive silver halide in the emulsion, a negative black-and-white image remains. The development process can be considered as a posterior amplification of the inherent photosensitivity. The larger the grains, the greater the amplification, but the lower the resolution. Holography usually requires high resolution and, hence, relatively low amplification.

In conventional photography, the exposure characteristics of the photographic emulsion are usually discussed in terms of a curve called the Huerter-Driffield (H-D) curve, which is a plot of the optical density versus the common

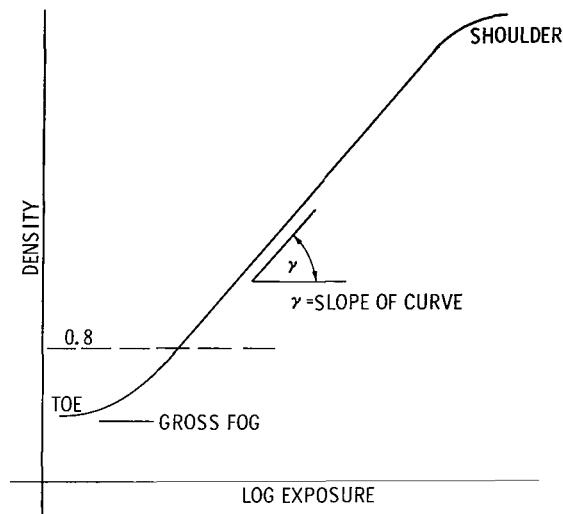log of the exposure. A typical plot of the H-D curve is given in Figure A-2.

In conventional photography, this characteristic curve contains all the necessary information on its response to exposure. This curve is constructed by exposing the film to a stepped function of exposure and plotting the resulting densities against these steps. The densities are measured with a densitometer calibrated to read logarithms to base 10 of opacity or reciprocal transmittance. The linear portion of this H-D curve is often called the range for correct tone reproduction. Staying on the linear portion of this curve allows an interpretation of the effect of the photographed gamma on the holographic process. In Figure A-2, this gamma is the slope of the linear portion of this curve. For the case of Fresnel and Fraunhofer holography, gamma, γ, appears as a parameter affecting the contrast of the reconstructed image.

Figure A-2. Characteristic curve

Observe here that this gamma (γ) is the one described in equation (11) of Section III.A. For a given material, the value of γ can be controlled by changing the type of developer and the time of development. It is pointed out here that all the holograms developed in the present experiment were carefully processed as follows:

1. Developer — D-19.

2. Development time — 5 min.

3. Stop bath — 0.5 min.

4. Fixer — 4 min.

5. Wash — 15 min.

6. Photo-flow — 0.5 min.

7. Chemical temperature — 20° (68°F).

8. Density — 0.8.

All photographs of the hologram image were processed just as carefully.

Characteristic curves contain much useful information in the case of certain holographic exposures; yet, still another curve exists that is quite useful. Recently, the amplitude transmission curves have been preferred because the local amplitude transmission, rather than the local density, is the more important consideration. A typical plot of this amplitude transmission factor is plotted against energy in ergs/cm^2 for a 10-E-75 Agfa Gavaert plate. The amplitude transmission factor is defined as the ratio between the amplitudes of a monochromatic plane wave after and before passing through the photographic emulsion. Now, the intensity transmission that was useful in the H-D curve is related to the transmission amplitude factor by:

$$T = T_a T_a^* = |T_a|^2 \qquad .$$

Therefore, since

$$T = (It)^{-\gamma} \qquad ,$$
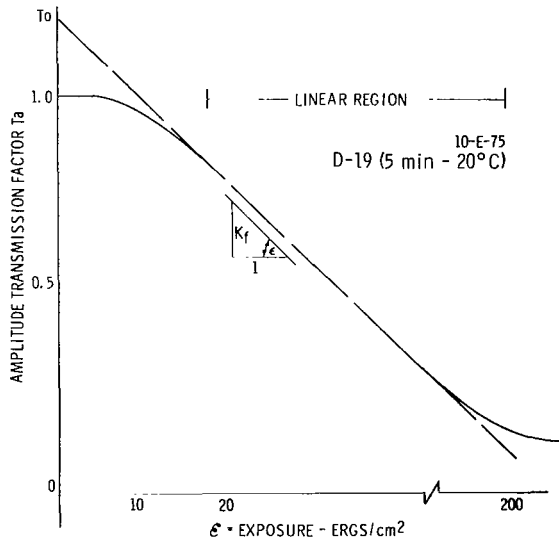
$$T_a = (It)^{-\gamma/2}$$

Figure A-3. 10-E-75 Amplitude
   transmission curve

Referring to Figure A-3, an expression used in equation (72a) is derived that is used repeatedly in the theory:

$$T_a = T_o - k_f \mathcal{E} \qquad .$$

From the m formula for the slope of a straight line,

$$m = \tan \epsilon = \frac{y_2 - y_1}{x_2 - x_1} \qquad ,$$

and Figure A-3, one may write:

$$\frac{k_f}{1} = \tan \epsilon = \frac{T_o - T_a}{\mathcal{E}}$$

79

as

$$k_f \, \mathcal{E} = T_o - T_a$$

or

$$T_a = T_o - k_f \, \mathcal{E} \quad ,$$

where k_f is the slope of the linear region of the curve and is determined by the film type and development time.

More should be said concerning the reciprocity of an emulsion. For a density of , say, 0.8, an exposure of approximately 20 to 50 ergs/cm^2 will suffice for non-Q-spoiled pulse (in the nanosecond range), reciprocity losses are such that to achieve the density of 0.8, the energy density for the exposure must be multiplied by a factor of approximately 2 to 4. It is sufficient to say that very short nanosecond-type pulses are much less efficient in their ability to expose the grains of emulsions. Figure A-4 is a photograph of an actual hologram such as that resulting from the experimental work done for this project.

Figure A-4. Photograph of hologram

REFERENCES

1. Horman, Melvin H.: An Application of Wavefront Reconstruction to Interferometry. Appl. Opt. vol. 4, no. 3, March 1965.

2. Rogers, G. L.: The Design of Experiments for Recording and Reconstructing Three-Dimen. onal Objects in Coherent Light (Holography). J. Sci. Instr., vol. 43, 1966.

3. Brooks, R. E., and Heflinger, L. O., et al.: Holographic Photography of High-Speed Phenomena with Conventional and Q-Switched Ru y Laser. Appl. Phys. Letters, vol. 7, no. 4, August 1965.

4. De Bitetto, D. J.: On the Use of Moving Scatterers in Conventional Holography. Philips Laboratories, Briarcliff Manor, New York, January 1966.

5. Forney, M. E., and Matkin, J. H., et al.: Aerosol Size and Velocity Determination via Holography. Rev. of Sci. Instr., vol. 40, no. 2, February 1969.

6. La Macchia, J. T., and Bjorkholm, J. E.: Resolution of Pulsed Laser Holograms. Appl. Phys. Letters, vol. 12, no. 2, January 1968.

7. Lehmann, Matt: Photography for Optical Measurements. Stanford University, Palo Alto, California, April 1967.

8. Leith, E. N., and Upatnieks, J., et al.: Hologram Visual Displays. J. Soc. of Mot. Pic. and TV Engns., vol. 75, no. 4, April 1966.

9. Long, Leslie T., and Parks, John A.: Simple Flash Holography. Appl. Opt., vol. 8, no. 5, May 1969.

10. Staselko, D. I., and Smirnov, A. G., et al.: Production of High-Quality Holograms of Three-Dimensional Diffuse Objects with the Use of Single-Made Ruby Lasers. Acquisition No. VDC 535.317.1, March 1968.

11. Stroke, George W.: A Reformulated General Theory of Holography. Presented at Symposium of Modern Optics Polytechnic Institute of Brooklyn, March 22-24, 1967.

REFERENCES (Continued)

12. Dyes, W. A., and Kellen, P. F., et al.: Velocity Synchronized Fourier Transform Hologram Camera System. Appl. Opt., vol. 9, no. 5, May 1970.

13. Goodman, J. W.: Temporal Filtering Properties of Holograms. Appl. Opt., vol. 6, no. 5, May 1967.

14. Hilderbrand, B. P.: A General Analysis of Contour Holography. NASA Acquisition No. AD 828 931, February 1968.

15. Leith, Emmett N., and Upatnieks, Juris: Reconstructed Wavefronts and Communication Theory. J. Opt. Soc. Am., vol. 52, no. 10, October 1962.

16. Neumann, Don B.: Holography of Moving Scenes. J. Opt. Soc. of A., vol. 58, no. 4, April 1968.

17. Brooks, R. E., and Heflinger, L. O., et al.: Interferometry with a Holographically Reconstructed Comparison Beam. Appl. Phys. Letters, vol. 7, no. 9, November 1965.

18. Chau, Henry H. M., and Horman, Melvin H.: Demonstration of the Application of Wavefront Reconstruction to Interferometry. Appl. Opt., vol. 5, no. 7, July 1966.

19. Dotson, William P., Jr.: In Effect of Object Motion in Fraunhofer Holography with Application to Velocity Measurements. NASA Report TN 9637, Washington, D. C., November 1969.

20. Born, M., and Wolf, E.: Principles of Optics. New York and London: Pergamon Press, 1967, Third Edition.

21. Goodman, J. W., and Knight, G. R.: Effects of Film Nonlinearities on Wavefront-Reconstruction Images of Diffuse Objects. J. Opt. Soc. of Am., vol. 58, no. 9, September 1968.

22. Friesem, A. A., and Zelenka, J. S.: Effects of Film Nonlinearities in Holography. Appl. Opt., vol. 6, no. 10, October 1967.

REFERENCES (Concluded)

23. Heflinger, L. O., and Wuerker, R. F., et at.: Holographic Interferometry. J. Appl. Phys., vol. 37, no. 2, February 1966.

24. Kurtz, Robert L.: Multiple Image Storing System for High Speed Projectile Holography. NASA Case No. MFS-20596, August 1969.

25. Kurtz, R. L., and Norden, B. N.: Hybrid Holographic System. U. S. Patent No. 3,535,014, November 1970.

26. Leith, Emmett N., and Upatnieks, Juris: Wavefront Reconstruction with Diffused Illimination and Three-Dimensional Objects. Opt. Soc. Am. vol. 54, no. 11, November 1964.

27. Reynolds, G. O., and Develis, J. B.: Hologram Coherence Effects. IEEE Transaction on Antennas and Propagation, vol. AP-15, no. 1, January 1967.

28. Mees, Kenneth: The Theory of the Photographic Process. The Macmillan Company, New York, 1954.

29. Ramberg, E. G.: The Hologram — Properties and Applications. RCA Rev., December 1966.

30. Smith, Howard M.: Principles of Holography. Wiley Intersciences, New York, 1969.

31. Kurtz, R. L., and Loh, H. Y.: A Holographic Technique for Recording a Hypervelocity Projectile with Front Surface Resolution. Appl. Opt., vol. 9, no. 5, May 1970.

32. Falconer, David G.: Role of the Photgraphic Process in Holography. Phot. Sci. Eng., vol. 10, no. 3, May–June 1966.

BIBLIOGRAPHY

Brooks, R. E., and Heflinger, et al.: Holographic Photography of High-Speed Phenomena with Conventional and Q-Switched Ruby Lasers. Appl. Phys. Letters, vol. 7, no. 4, August 1965.

Caulfield, H. J., and Lu, Sun, et al.: Biasing for Single-Exposure and Multiple-Exposure Holography. Letters to the Editor, Appl. Opt., vol. 7, July 1968.

Collier, Robert J.: Holography and Integral Photography. Phys. Today, vol. 12, July 1968.

Frecska, Sandor A.: Characteristics of the Agfa-Gevaert Type 10E70 Holographic Film. Appl. Opt., vol. 7, no. 11, November 1968.

Friesem, A. A., and Zelenka, J. S.: Effects of Film Nonlinearities in Holography. Appl. Opt., vol. 6, no. 10, October 1967.

Goodman, J. W., and Miles, R. B., et al.: Comparative Noise Performance of Photographic Emulsions in Holographic and Conventional Imagery. J. Opt. Soc. of Am., vol. 58, no. 3, May 1968.

Goodman, J. W.: Film-Grain Noise in Holography. Presented at Symposium on Modern Optics — Polytechnic Institute of Brooklyn, March 22-24, 1967.

Lurie, M.: Effects of Partial Coherence on Holography with Diffuse Illumination. J. Opt. Soc. Am., vol. 56, no. 10, October 1966.

Mau, Allan E., and Young, Willard A.: An Electronic Shutter for Holographic Applications. Appl. Opt. vol. 7, no. 7, July 1968.

Paques, H., and Smigielski, P.: Holography. NASA TN-8506, August 1966.

Pistol kors, A. A.: Resolving Power of a Hologram. Sov. Phys. Dokl., vol. 12, no. 1, July 1967.

Redman, J. D.: Holographic Velocity Measurement. J. of Sci. Instr., vol. 44, 1967.

Siebert, L. D.: Front-Lighted Pulse Laser Holography. Appl. Phys. Letters, vol. 11, no. 10, November 1967.

Trolinger, J. D., and Farmer, W. M., et al.: Multiple Exposure Holography of Time Varying Three-Dimensional Fields. Appl. Opt., vol 7, August 1968.

"The aeronautical and space activities of the United States shall be conducted so as to contribute . . . to the expansion of human knowledge of phenomena in the atmosphere and space. The Administration shall provide for the widest practicable and appropriate dissemination of information concerning its activities and the results thereof."

— NATIONAL AERONAUTICS AND SPACE ACT OF 1958

NASA SCIENTIFIC AND TECHNICAL PUBLICATIONS

TECHNICAL REPORTS: Scientific and technical information considered important, complete, and a lasting contribution to existing knowledge.

TECHNICAL NOTES: Information less broad in scope but nevertheless of importance as a contribution to existing knowledge.

TECHNICAL MEMORANDUMS: Information receiving limited distribution because of preliminary data, security classification, or other reasons.

CONTRACTOR REPORTS: Scientific and technical information generated under a NASA contract or grant and considered an important contribution to existing knowledge.

TECHNICAL TRANSLATIONS: Information published in a foreign language considered to merit NASA distribution in English.

SPECIAL PUBLICATIONS: Information derived from or of value to NASA activities. Publications include conference proceedings, monographs, data compilations, handbooks, sourcebooks, and special bibliographies.

TECHNOLOGY UTILIZATION PUBLICATIONS: Information on technology used by NASA that may be of particular interest in commercial and other non-aerospace applications. Publications include Tech Briefs, Technology Utilization Reports and Technology Surveys.

Details on the availability of these publications may be obtained from:

SCIENTIFIC AND TECHNICAL INFORMATION OFFICE

NATIONAL AERONAUTICS AND SPACE ADMINISTRATION
Washington, D.C. 20546